Deciphering Photosynthetic Protein Networks: A Crosslinking-MS Strategy for Studying Functional Thylakoid Membranes

Nicolas Frances[1,2], Cecile Giustini[1], Giovanni Finazzi[1], Myriam Ferro[2], Pascal Albanese[1,2*]

1. PCV-LPM, UMR5168/UMR1417 UGA-CNRS-CEA-INRAe. 17 Avenue des Martyrs, 38054 Grenoble, France
2. BGE-EDyP, U13 UGA-CEA-Inserm / UAR2048 -CEA CNRS. 17 Avenue des Martyrs, 38054 Grenoble, France

*pascal.albanese@cea.fr

Abstract

Photosynthesis, which sustains life on Earth, depends on highly organized yet adaptable protein assemblies embedded in specialized membranes called thylakoids. Understanding how protein complexes dynamically interact within functional photosynthetic membranes is critical for elucidating cellular energetic metabolism. Here, we present an improved crosslinking mass spectrometry (XL-MS) strategy that captures native protein interactions in functional, photosynthetically active thylakoid membranes from Arabidopsis and Spinach. By monitoring photo-physiology parameters, we demonstrate that electron transport remains physiologically active during the crosslinking process, enabling structural interrogation without disrupting native organization. Mapping crosslinks onto known structures confirms the structural integrity of major complexes and highlights previously uncharacterized assemblies. Our findings pave the way for exploring membrane protein networks *in situ* and set the stage for integrative structural studies of photosynthetic regulation and adaptation.

Introduction

Evolution has produced along billion years of evolution a variety of complex sub-cellular compartments inside living cells. Within each, proteins perform biochemical functions as part of macromolecular assemblies, these in turn form large network of molecular interactions within a cell, referred to as its interactome. . Energy metabolism in eukaryotic cells also rely on a dynamic network of protein complexes embedded in the membranes of specialized organelles the ubiquitous mitochondria and, in oxygenic eukaryotic phototrophs, the chloroplasts. Oxygenic photosynthesis has driven nearly all life forms on Earth since over 3.5 billion years, using Sunlight as the energy source, thus coping with its variability in intensity and quality across nearly every habitat (Blankenship 2010). This remarkable adaptability lies with complex regulatory networks inside the chloroplast thylakoid membranes where highly conserved catalytic cores, the photosystems (PS) I and II, work in series with the Cytochrome b_6f and ATP synthase complexes (Eberhard et al. 2008). Opposed to the overall evolutionary conservation of these major complexes, several proteins interacting with them, stably or transiently, have been the evolutionary key in photosynthetic adaptation, both for harvesting sunlight in form of external antenna systems (Croce and van Amerongen 2020) and mitigating its harmful effects through photoprotective mechanisms (Bassi and Dall'Osto 2021). The cellular interactome can adapt much faster to

environmental cues than the transcriptome or the proteome (Bludau and Aebersold 2020), and its changes represent therefore a major target to understand how organisms adapt to environmental cues. These organisms power our society, from oil and coal to our main food crops, our energy supply is based on the productivity of photosynthetic life. Consequently, understanding the dynamic network of native thylakoid interactions is key to meet future needs and develop new technologies (Ray et al. 2013), understanding the photosynthetic thylakoid's interactome dynamics in a near-native and functional state is of primary importance to meet future challenges (Ort et al. 2015).

Multiple techniques developed in recent years have enable the detection and visualization of protein networks and their architectures, often retaining the cell's native or near-native environment (McCafferty et al. 2024). These include light expansion microscopy, cryo-electron microscopy and tomography (cryo-EM/ET), and mass spectrometry (MS) (Klykov et al. 2022; Kelley et al. 2024). For cryo-EM/ET approaches the major limitations is the need of biochemical purification (Cryo-EM single particle) and sample snap-freezing prior to analysis, sometimes with long procedures and difficult access to state-of-the-art technical facilities (Beck and Baumeister 2016). For MS-based analysis, it's necessary to denature and digest samples prior to data acquisition (McCafferty et al. 2024). For any approach, limitations are exacerbated when analyzing membrane proteins. It appears clear that a multifaceted approach combining spatial organization with functional and molecular identity will be key to understand biological complexity across scales.

A promising approach to study protein-protein interactions across several scale of complexity is crosslinking (XL) coupled to MS (Chavez et al. 2018; O'reilly and Rappsilber, n.d.). The approach relies on the use of chemical crosslinking reagents forming covalent bonds between amino acids in close spatial proximity. Once the two crosslinked peptides are sequenced by MS, they yield a distance restraint, typically between 6 and 35 Å, at the residue level (Belsom and Rappsilber 2021). These are particularly suitable to be fruitfully integrated with cryo-ET and cryo-EM imaging (Kastritis et al. 2017; O'Reilly et al. 2020; Mosalaganti et al. 2022; Albanese, Tamara, Saracco, et al. 2020).

The use of XL is not new in plant biochemistry (Baird and Hammes 1976; Henriques and Park 1978), but the increasing sensitivity of MS instruments has allowed an increasing yield of reliable identifications. The gain in popularity of XL-MS is indeed mainly due to its relatively ease of use, robustness, increasing availability of crosslinking reagents with adaptable chemistry (Steigenberger et al. 2020) and the recent integration with cryo-ET/EM and AI-driven structure prediction tools, where XL-MS can serve as both validation (Burke et al. 2023) and to drive the prediction. So far, limiting factors for proteome-wide studies have been mostly the high dynamic range of cellular proteomes (Chavez et al. 2019; Liu et al. 2018), requiring extensive fractionation and long MS acquisition times. In addition, a non-negligible limitation is that it may not yield physiologically relevant structural information due to the covalent bonds formed during the reaction. Several attempts have been undertaken to identify the sub-cellular interactome of mitochondria (Hevler et al. 2023; Liu et al. 2018) and eukaryotic cells (Kastritis et al. 2017) while only few examples exists for plants chloroplasts/thylakoids (Albanese, Tamara, Scheltema, et al. 2020; Ditz et al. 2024; Weisz et al. 2017) or microalgae. XL-MS provides a powerful approach that can be applied holistically without a predefined target, with incubation times as short as 20 minutes. From a structural modelling standpoint, it also allows to retrieve precise spatial constraints (*e.g.* 6-35 Å) to model protein-protein interaction interfaces and dynamics (Mendes et al. 2019; Bar Barroeta et al.

2024). So far, no XL-MS study has been coupled to functional measurements to prove it can yield physiologically relevant results.

In this study, we developed a fast and reproducible pipeline that improves cross-linking efficiency in functional thylakoid membranes extracted from two plant species: *Spinacia oleracea* (Spinach) and *Arabidopsis thaliana.* The main advantage of using functional thylakoid membranes is that we are able to measure the physiological impact of chemical crosslinking *in situ* during the reaction. We used an enrichable cross-linking reagent (disuccinimidyl phenyl phosphonic acid, or PhoX) to generate a robust and reproducible output with hundreds of unique crosslinks within few hours of MS-acquisition, allowing to go from sample-to-data in ~3 days for several replicates and conditions. We showed that, even increasing the crosslinker/sample ratio, we retain at least half of the photosynthetic activity during the 30 minutes of crosslinking reaction when compared to control samples, demonstrating the physiological relevance of the structural information extracted. We also tested the combination of Phox with trimethylphenylammonium chloride (TMPAC), showing that it is possible to increase the yield of relevant crosslinks without hampering the physiological context. In conclusion, of dozens of novel protein-protein interactions detected, we provide structural model for putative novel functional complexes. We believe/conclude that this workflow will pave the way for integrative studies on functional membranes systems and bioenergetics organelles, beyond photosynthesis research.

Results and Discussion

`

Establishing a Physiological Benchmark for *In Situ* Structural Proteomics of Functionally Active Thylakoid Membranes

Studying protein interactions within native biological membranes presents a formidable challenge due to the need to preserve the delicate structural and functional context of the system. Multiple crosslinking reagents have been developed to cover specific constraints in interaction distances and aid during MS identification (Belsom and Rappsilber 2021). PhoX is a functionalized crosslinker with a phosphonic group, which allows peptide enrichment by immobilized metal-affinity chromatography (IMAC, Steigenberger et al. 2019). This same negatively charged functional group is however believed to cause its cell-impermeability (Steigenberger et al. 2019), which has been reported to be repelled by biological membranes (Vedadghavami et al., 2020). This might reduce PhoX crosslinking efficiency due to coulombic repulsion from exposed acidic amino acids (Lyu et Lazár, 2022; Kaňa et Govindjee, 2016). To optimize PhoX application in thylakoids, we propose a pipeline incorporating TMPAC, an amphiphilic ammonium salt. Its cationic group may neutralize surface charges, allowing PhoX proximity, and improving protein interaction capture. In the same context, we aim to evaluate the compatibility of TMPAC and Phox with thylakoid structural integrity and photosynthetic performances.

To assess whether our crosslinking protocol maintains physiological integrity, we measured photosynthetic activity proxies: the maximum quantum yield of PSII (Fv/Fm) and Electron Transport Rate (ETR) in thylakoid membranes treated with crosslinkers, with and without adjuvant chemical molecules (*i.e.* TMPAC). We first combined confocal imaging of isolated thylakoids upon chemical crosslinking treatment (with and without TMPAC) and functional measurement of photosynthetic electron flow by chlorophyll fluorescence. This allowed us to establish an optimized protocol for the

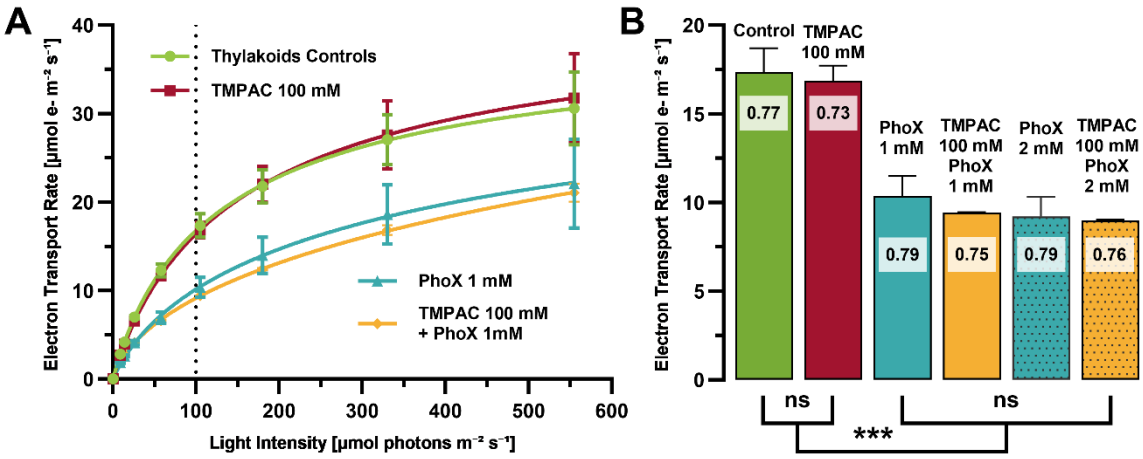

Figure 1. Photosynthetic activity is partially retained during crosslinking of functional thylakoid membranes. (A) Electron transport rate (ETR) curves of spinach thylakoids under increasing light intensity show how crosslinking with PhoX affects photosynthetic performance. (B) ETR values under moderate light (105 µmol photons m^{-2} s^{-1}, dashed line in panel A) are plotted for multiple treatment conditions. PSII quantum efficiency in the dark (Fv/Fm) is also reported overlayed to the bar in a textbox (complete values in Figure S2).

isolation of functional thylakoids from both model organisms., Purified thylakoids retain intact grana and thylakoid organization and most also retain the envelope (**Figure S1**), as also shown by recent reports (Bos et al. 2023; Berentsen et al. 2025).

To examine photosynthetic electron transport under light, we measured ETR at increasing light intensities up to 600 µmol photons m^{-2} s^{-1} (**Figure 1A**). First, a titration of increasing Phox and TMAPC concentrations on both species showed that even very low amounts of crosslinker impair the photosynthetic electron transport (**Fig. S2**). On the other hand, TMPAC addition up to 100mM did not affect the ETR, and shows no addictive effect when used in combination with Phox. In both Spinach and *Arabidopsis* thylakoids, PhoX at 1 or 2 mM reduced ETR by half, indicating partial inhibition of electron flow (**Fig.1A and Fig. S2**). This effect is likely due to covalent spatial crosslinking of electron transport-associated proteins, and possibly the chemical modification via the NHS ester labelling of key lysine residues of PsaC (Fischer 1998) and cytochrome b_6f (Gong et al. 2000). The addition of an amphiphilic cation, TMPAC, did not significantly affected the ETR when combined with PhoX. Arabidopsis thylakoids treated with PhoX and TMPAC showed a 52% ± 13% decrease in ETR, only marginally lower than with PhoX alone (44% ± 10%). This reduction occurred without drastic alterations in the PSII quantum yield in the dark (Fig. 1B, and Fig. EV2C), suggesting that the interference in electron flow occurs during illumination, while in the dark the thylakoid membrane organization and PSII structural configuration remain largely preserved. We therefore decided to perform the subsequent experiments in dark-adapted conditions.

Since ETR reflects the overall electron flow under illumination across PSII, cytochrome B_6f and PSI, this suggests that only the crosslinking treatment perturbs the entire electron transport chain, yet retaining at least half of the functionality in all conditions tested. This can be expected since we introduce covalent bonds between proteins and electron carriers that need dynamic delocalization for

their functioning. However, the maximum quantum yield of PSII photochemistry (Fv/Fm, Figure 1B) remained largely unchanged in dark-adapted samples, indicating that PSII structural integrity was preserved in the dark. Therefore, we continued working with dark-adapted samples.

Altogether, these physiological measurements confirm the feasibility of the crosslinking approach on functionally active membranes—an essential step forward for membrane systems biology. They demonstrate that crosslinking can be performed on isolated thylakoids in near-native, physiologically active states. The next step is to evaluate the MS readout and the structural data that can be extracted, to detect structurally informative crosslinks under physiologically relevant conditions.

Increased Detection of Crosslinked Peptides Under Physiologically Optimized Condition

Mass spectrometry analysis of the crosslinked peptides identified a total of 832 and 828 unique crosslinks in Spinach (*So*) and *Arabidopsis* (*At*) thylakoids in a total of 8 independent experiment with 3 replicates each (Supplementary Table 2). Only crosslinks identified in at least 2 replicates were considered. The number of unique protein-protein pairs in this analysis was 233 and 410 for Spinach (So) and Arabidopsis (At), respectively. The addition of TMPAC increased the identification of crosslinked peptides across all experimental conditions (Figure 2), while not impacting the physiological state. The enhancement ranged from 3.8% to 55.7% for individual samples, with an average increase of 23.6% across two out of three replicates and 30.6% across three out of three replicates (Figure 2B).

While approximately half of the detected crosslinks are shared between the two treatments (Figure 2B) about one third of the crosslinks could only be identified upon TMPAC treatment when considering highly reproducible crosslinks. Indeed, considering only crosslinks detected in all 3 replicates, the proportion of total XLs and CSMs increased significantly in the TMPAC-treated samples, along with a rise in the number of crosslinks uniquely detected in the presence of TMPAC (Figure 2B). This suggests that TMPAC not only increases crosslinking yield but also enhances its reproducibility.

Overall, we identified hundreds of reproducible crosslinked peptides in a physiologically active sample, and in a rapid manner using the enrichable crosslinker Phox. The addition of TMPAC as an enhancer allows for the detection of 20-30% more reproducible crosslinks, and the characterization of 89 additional inter-protein pairs of the 214 total, a remarkable gain in informative protein-protein pairs.

.

Crosslink Distance Distributions Reflect Native-Like Architecture

PhoX-mediated crosslinking imposes a characteristic spatial constraint, generally falling within a range of 7 to 25 Å (see Figure 3), owing to the lengths of lysine side chains (7 Å), backbone flexibility (6 Å), and the crosslinker molecule (~7 Å). Accounting for structural flexibility and solvent accessibility, the experimentally verified upper limit is 33–35 Å (Bullock et al. 2018). Accordingly, we used this criterion to validate and map our crosslinking data onto available PDB structures for both plant systems. All the distances measured in know complexes of Spinach and Arabidopsis (8 and 5, respectively) are plotted in Figure 3A. As an example of mapping, we show the So_P1 crosslinks mapped onto the PSII-LHCII supercomplex structure (PDB #3JCU, Figure 3B)

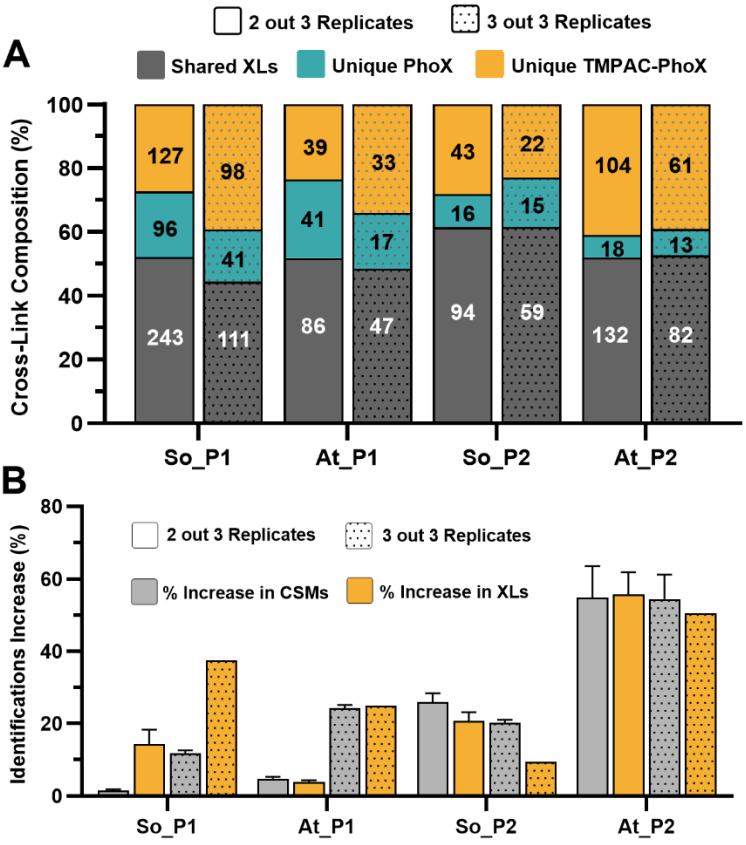

Figure 2. Enhanced detection of protein interactions within functional thylakoid membranes. A) Relative of identified crosslinks (XLs) and crosslink spectra matches (CSMs) found within replicates containing 100 mM TMPAC plus PhoX (1 mM and 2 mM as P1 and P2) with respect to the control condition (Only PhoX) in *A. thaliana* (At) and *S. oleracea* (So) thylakoids. Crosslinks uniquely found with only PhoX in control conditions in blue, those found in combination with TMPAC are presented in yellow, and common crosslinks in both treatments in gray. Numbers within each section represent total XLs counts. B) Stacked bar chart representing the number of crosslinks after filtering the hits by those found in 2 out 3 replicas (plain) and 3 out 3 replicas (dotted). Results

At 2 mM PhoX, longer-than-expected distances (>35 Å) were observed in *A. thaliana* and spinach (At_P2 and So_P2, Figure 3A). A smaller proportion of these outliers appeared in 1 mM PhoX-treated samples, particularly in spinach (So_P1), where most crosslinks remained within range. This may suggest that the treatment with 2 mM PhoX (P2) might not be the most appropriate, and 1 mM treatment (P1) may be preferable. Also, this difference might be favored by the additional washing steps after the crosslinking reaction (see Methods), which can remove abundant soluble proteins like RuBisCO and histones, as well as fragmented membranes.

Overall, over 97% of the detected crosslinks are within the expected distances for the 1 mM PhoX samples, and down to 85-90% for the 2 mM. This is consistent with the idea that higher crosslinker concentration may introduce longer or artifactual crosslinks (longer than the 35 Å cut-off, dashed line in Figure 3A) and that sample preservation can affect complex integrity. Importantly, the additional

TMPAC treatments did not increase these average distances (Fig. 3), *i.e.* it did not introduce artifacts. It is also worth noting that less than 10% of our data (84 out of 898 total peptide pairs for At and So) have structural matches in known experimental structures. This depends both on the relatively little amount of known structures for the model organism *A. thaliana* compared to Spinach, and on the tendency of yielding crosslinked peptides on flexible and solvent-exposed domains of proteins (*e.g*. N-terminal loops of Light-harvesting complexes) as previously reported (Albanese, Tamara, Saracco, et al. 2020). This also underlines the complementarity between the two approaches and the positive outcome of using XL-MS to complement other structural approaches to uncover novel functional protein complexes *in situ*.

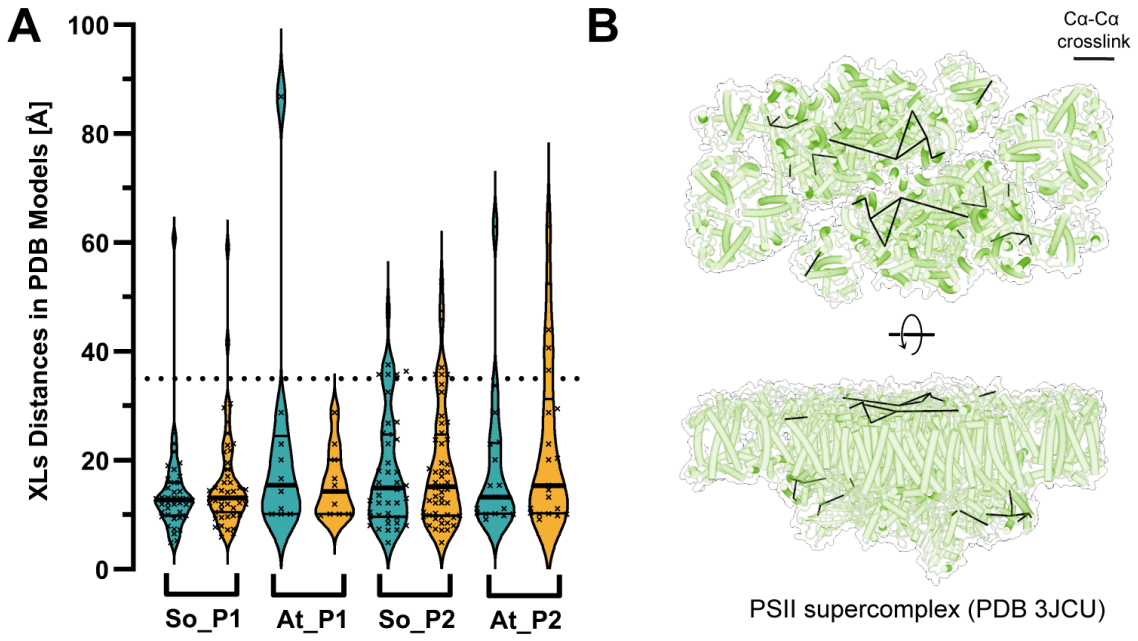

Figure 3. Structural validation of identified crosslinks by measuring distances in available PDB models of chloroplast protein complexes of spinach: 3JCU (PSII-LHCII), 6VON (Chloroplast ATP synthase), 7ZYV (Cytochrome B6f), 2WSC (PSI-LHCI), 7Q57 (GAPDH), 4V61 (Chloro-ribosome), 8RUC (RuBisCO), and 4RI2 (PsbS). In *A. thaliana*, five models were containing identified crosslinks: 7OUI (PSII-LHCII), 7WG5 (NDH-PSI-LHCI), 7UX9 (DDM1), 3RFY (Cyclophilin 38), and 5IU0 (RuBisCO). (A). Experimental conditions are separated by crosslinks found in *A. thaliana* thylakoids (At) or Spinach (So). Blue represents the control condition crosslinked with PhoX alone (1 mM and 2 mM as P1 and P2), and in yellow its combination with 100 mM TMPAC. If multiple subunits of the same protein were present in the PDB model, only the shortest crosslink was considered. The central mark indicates the mean value, with the quartiles as a thin line above and below. Each distance is represented by individual lines, and the horizontal line marks the maximum expected distance for 35 Å. (B) Example of PDB model of Photosystem II – LHCII supercomplex from spinach (3JCU) after fitting of all crosslinks (in black) found in So_P1 (2 out 3 replicates).

A Scalable Framework for Mapping Functional Membrane Protein Networks Beyond Known Complexes

Once we validated our approach from a physiological and structural point of view, we focused on the interactome landscape, chasing novel protein pairs and unexplored interactions. Maps, for both species, were generated to retain crosslinks detected in at least two or three replicates. For completeness 1 and 2 mM datasets, with and without TMPAC, are visualized together (separate maps can be explored from Extended Data 1). In Spinach thylakoids (*Arabidopsis* is in Figure EV4), --------

provides a complete overview of the reproducible protein-protein interactions identified in this study, along with curated protein names (see Supplementary Table 3 for Uniprot and gene name mappings). The primary protein interaction networks involved PSII components, along with ATP synthase, Photosystem I (PSI), and, to a lesser extent, cytochrome b_6f (Figure 4 and EV4). The identified crosslinked proteins could be categorized into three main groups: 1. well-characterized proteins complexes of the photosynthetic electron transport chain (*e.g.* PSII, PSI and their LHC) which are established components of mature complexes with known structural data. These proteins are colored based on the complex that they belong to, or are functionally associated to (Figure 4 for So and EV4 for At). 2. Adjuvant or regulatory protein, , such as those containing functionally associated domains like LHC-like proteins (*e.g.* LIL, PsbS) and annotated functions like peptidyl-prolyl isomerases (PPIases). 3. The third group comprises uncharacterized or predicted proteins, including plastid-lipid-associated proteins (PLAPs), for which little to no functional information is available, or can be ambiguous. This expanded protein interaction network offers a more comprehensive view of chloroplast protein organization, potentially revealing previously unknown functional relationships. All these maps are interactively accessible in the crosslinkviewer.net web application through the Supplementary Data 1.

Crosslinking MS provides distance constraints that are useful for predicting and validating structural models generated *in silico* (Graziadei and Rappsilber 2022; Burke et al. 2023). In this study we detected a relevant number of protein-protein interactions that belongs to proteins with either a functional characterization but not a known structure, or neither of both (Figure 4). We hereby highlight a few examples based on their relevance to answer long standing questions in the field, or open new potential paths for uncovering the function of previously uncharacterized proteins.
Among several PSII interactors we could identify a previously characterized protein named **FIP** (Figure 5, bottom-left)**.** Its knockdown mutant has an increased resistance to high light conditions (Lopes et al. 2018). Here, we show that FIP interacts via its stromal flexible loop with the PsbD and PsbE components of the PSII reaction center (Figure EV4). Such an interaction was never described, therefore we predicted the FIP-PsbD-PsbE structure using the alphafold3 server (Abramson et al. 2024). The predicted modelis well supported by our experimental results, with all mapped distances within 35 A (PDB models in Source Data). Due to FIP's predicted function as a protein interacting with FtsH proteases (Lopes et al. 2018), it is tempting to suggest its function as a mediator of PSII disassembly.

A common characteristic of uncovered interactors is the predominant targeting of intrinsically flexible regions or disordered regions. For instance TSP9, a thylakoid soluble phosphoprotein, is reproducibly crosslinked to the PetD N-terminus of the cytochrome B6f. Previous work has proposed that TSP9

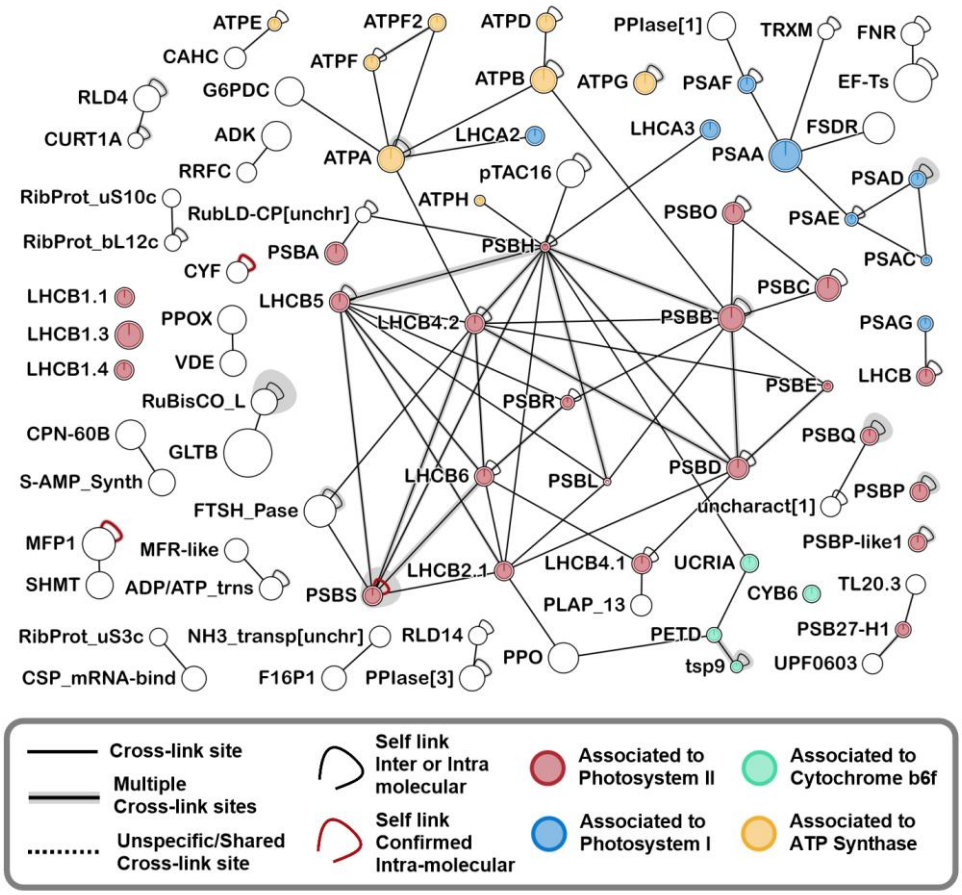

Figure 4 Interactome overview of thylakoids extracted from high-light Spinach acclimated leaves (450 µmol photons m^{-2} s^{-1}) crosslinked with 1 mM of PhoX crosslinker (with and without TMPAC). XLs present in at least 2 out of 3 replicas for each treatment are shown. Crosslink sites refers to dipeptides covalently bound; further details can be seen by opening the Supplementary Data in the web application https://crosslinkviewer.org . Color coding of the proteins are based on the information available about their known interaction with photosynthetic complexes, or during their assembling. Due to the complexity in multi-interactions given by LHCB1 antenna proteins, these are not shown here (full view of the interactome in Extended Data 1)
LHCII supercomplex from spinach (3JCU) after fitting of all crosslinks (in black) found in So_P1 (2 out 3 replicates).

regulates light harvesting facilitating the dissociation of LHCII from PSII (Hansson et al. 2007; Fristedt et al. 2009). Here we show the reproducible detection of Tsp9 bound to PetD of the cytochrome B6f complex. This finding is in agreement with the presence of a rather small stretch of sequence of this subunit in a recent structure of cytochrome B_6f (Sarewicz et al. 2023), and its possible absence in others due to a weaker interaction, which could be lost upon solubilization. Overlaying the predicted alphadfold2 structure (Jumper et al. 2021) of Spinach TSP9 with the cryo-EM structure (PBD 7ZYV) of the cytochrome, we can show that 3 out of 4 inter-protein crosslinks with PetD are slightly longer than

the threshold distance of 35 Å, namely between intrinsic disorder regions of TSP9 C-terminus. Our results confirms that TSP9 is part of the cytochrome b_6f, at least in dark adapted thylakoids,

Among the various modes of chloroplast electron transport, regulation often occurs at the level of Photosystem I (PSI), where pathways like cyclic electron flow (CEF) and the water–water cycle modulate energy production and redox balance. The latter contributes to ROS formation, as photoreduction at PSI generates superoxide, which is rapidly converted to H_2O_2 (Asada 1999). Detoxification relies on

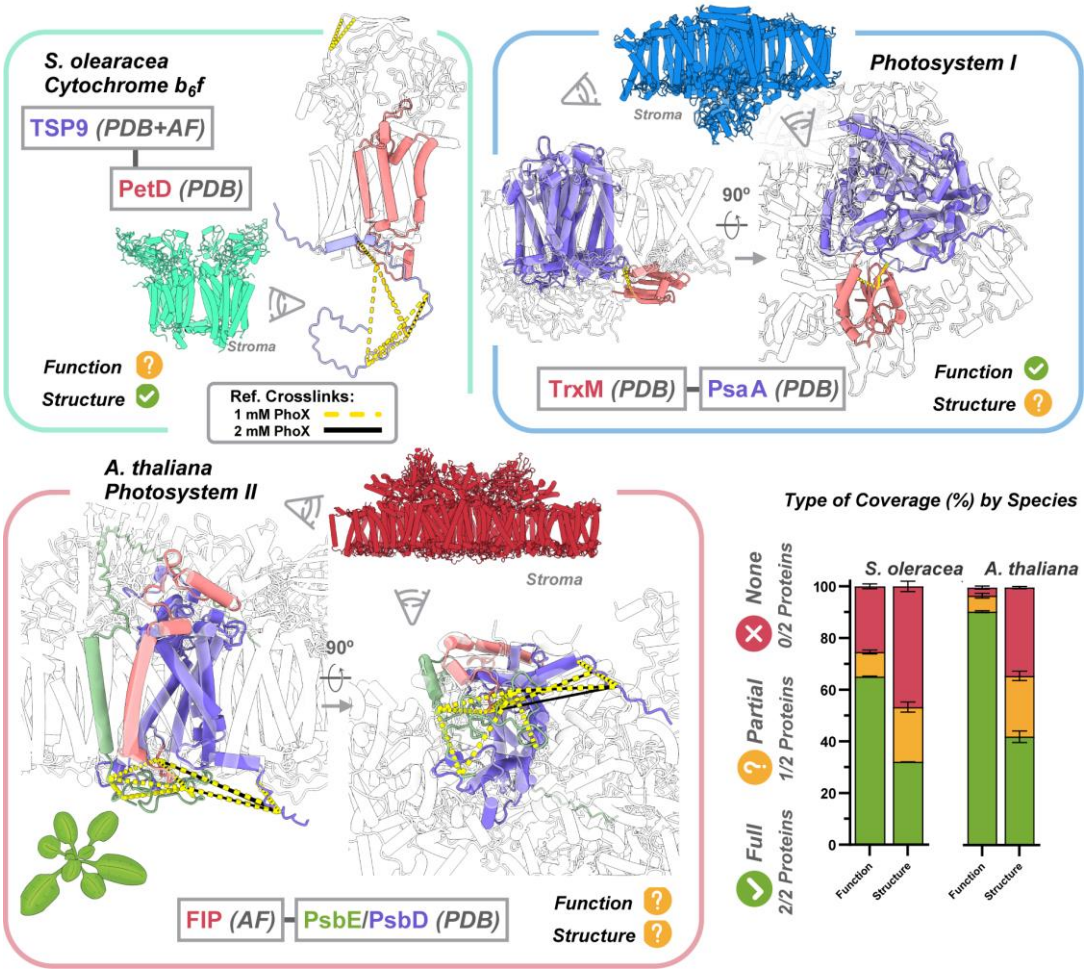

Figure 5. Structural and functional mapping of crosslinked protein interactions in *Spinacia oleracea* and *Arabidopsis thaliana*.

Representative examples of crosslinks detected between photosynthetic complexes and associated proteins, shown in structural models of PSII, PSI, cytochrome B_6f, and their interacting partners. Highlighted interactions include TSP9–PetD (So) and PsaA–TrxM (So), as well as FIP–PsbE/PsbD (At). Crosslinks are displayed as yellow dashed lines. Bar plots (right) summarize the proportion of detected protein pairs with full (green), partial (orange), or no (red) annotation in terms of structural (PDB coverage) and functional (UniProt annotation) information across both species and PhoX concentrations (1 mM, 2 mM).

enzymes such as ascorbate peroxidases (APXs), catalases, and thioredoxins (TRXs) (Schürmann and Buchanan 2008; Courteille et al. 2013).

Here, we observed two notable spatial associations of Thioredoxin M (TRXM) with the PSI core subunit PsaA (Figure 5). The two interlinks found fit the *in silico* docked model. This proximity in dark-adapted thylakoids may suggest a localized redox relay, allowing TRXM to rapidly modulate PSI activity linked to ferredoxin (Dai et al. 2007).

Conclusions

This study establishes a robust and physiologically grounded approach to probe membrane protein interactions in functional thylakoid membranes using chemical crosslinking coupled to mass spectrometry. By demonstrating that photosynthetic activity is only partially affected during crosslinking, we show that structural proteomics can be applied directly to intact, light-responsive membranes — a critical advance for studying complex macromolecular assemblies *in situ*. . To our knowledge, the present work is the first example of the use of XL-MS on a purified bioenergetic membrane system in close-to-native and functional conditions.

The use of PhoX, in combination with a charge-masking molecule (TMPAC), expands the detectable crosslink landscape without compromising physiological relevance. The resulting data reveal several reproducible interactions, and new contacts between core photosynthetic complexes, assembly and repair factors, and previously uncharacterized proteins. Structural validation across known 3D models confirms that most crosslinks fall within spatial constraints, and interactome maps illustrate dynamic connectivity across traditionally compartmentalized thylakoid domains.

Overall, we conclude that XL-MS is a powerful tool to bridge functional and structural biology in plants, enabling the systematic exploration of protein networks under functional conditions. Our workflow is rapid, reproducible, and adaptable, offering a practical framework for investigating plastid biogenesis, energy metabolism, and stress responses in photosynthetic systems. Looking ahead, the integration of this approach with quantitative crosslinking, cryo-EM, and machine-learning-based structural modeling will provide unprecedented insight into the organization and regulation of energy-converting organelles.

Materials and Methods

Thylakoid Membrane Extraction

Wild type plants of *Arabidopsis thaliana* (At) and *Spinacia oleracea* (So) cultivar 'Paris HF1' (Vilmorin), were grown at 22°C with a 12/12-hour light/dark cycle and a light intensity of 100 µmol m^{-2} s^{-1} for about six weeks. To perform "High-Light" treatment, plants were transferred to a growing chamber with an illumination of 450 µmol photons m^{-2} s^{-1} for 10 days. Leaves were harvested in a cold chamber at 4 °C under dim green light at the end of the night cycle. The leaf tissues were ground in a

blender using a base buffer containing 20 mM HEPES pH 8, 5 mM MgCl2, 22 mM KCl, and 10 mM NaCl, with an additional 0.3 M of sucrose. For every 50 g of *A. thaliana* leaves (At), 900 mL of buffer was used, and 100 g for spinach leaves (So) for the same buffer volume. The plant material was blended in 15 separated pulses of about 1 second each. The resulting paste was filtered through a quadruple-layered cheesecloth and centrifuged at 3000g for 5 min. The pellet was resuspended in the same base buffer supplemented with 0.1 M sorbitol. The chlorophyll content was measured by diluting thylakoids in 80% acetone, as described by Porra et al. (2018). The samples were stored adding 1 M betaine (CAS:107-43-7) in the same resuspension buffer (in the dark), then quickly frozen in liquid nitrogen and eventually stored at −70 °C. For samples At_P1 and So_P1 and samples prepared for confocal imaging, thylakoids were used directly for the experiments, without freezing.

Confocal Microscopy Imaging

Imaging was performed using a Zeiss LSM 900 confocal microscope equipped with ZEN software (version 3.0, Blue edition) with minor modification from previous set-up (Giustini et al. 2025). A 63x/1.4 M27 objective lens was used in confocal mode with an Airyscan 2 detector to ensure fast acquisition without compromising sensitivity, aided by a collimation optic. Excitation for chlorophyll fluorescence was provided by a 405 nm blue laser, and emission was collected between 650 and 700 nm. Nile Red visualization involved 488 nm excitation with fluorescence collected between 557 and 592 nm.

Determination of the Maximum Quantum yield of PSII and Thylakoid Photosynthetic Activity

To evaluate the effects of TMPAC on thylakoid membranes during photochemistry, we measured the maximum quantum yield of PSII (Fv/Fm) and the photosynthetic electron transport rate to assess photosynthetic efficiency. Photosynthetic electron flow was examined under several conditions: only thylakoids (control), 100 mM TMPAC, 1 mM PhoX, 2 mM PhoX, and combinations of PhoX with TMPAC.

Chlorophyll fluorescence was quantified using a Speedzen III fluorescence imaging setup (JBeam Bio, France). Maximum fluorescence (Fm) was determined by saturating red pulses (520 nm, 250 ms, 3000 µmol photons m^{-2} s^{-1}) and 10 µs detection pulses of blue light (470 nm). Minimum fluorescence in the dark was determined by using the same detection pulses in the absence of saturating pulses (F0) The maximum quantum yield of PSII was calculated as Fv/Fm=(Fm-F0)/Fm (Maxwell and Johnson 2000). The electron transport rate (ETR) was measured using the same setup and increasing the intensity of a continuous light at different light intensities after every 5 minutes of illumination for a total measurement time of 40 minutes (including a 5 minute of dark period to evaluate sample recovery.

Experimental Setup for Protein Cross-linking

Thylakoid solutions were treated with addition of 1 or 2mM PhoX (100 mM stock solution in anhydrous DMSO) or in combination with 100 mM TMPAC (1M stock solution in water). Detailed conditions are in Supplementary Table 1. Four experimental conditions were set, the combination of At and So with PhoX 1 mM (P1) and 2 mM (P2), denominated as At_P1, At_P2, So_P1, So_P2. The reaction mix was kept in the dark at room temperature, and it was stopped after 30 minutes with 50 mM NH_3. An extra step of thylakoid washing was performed in At_P1 and So_P1 to remove non-membrane proteins. These samples were centrifuged at 3000×g for 5 min, resuspended in 1 mL of only base buffer, and centrifuged again before final resuspension in 300 µL of fresh base buffer. Another crucial aspect is that P1 treatment of crosslinking was performed the same day of extraction before betaine quick freezing, and this might impact in the stability of thylakoid membranes.

Total protein was precipitated by adding ice-cold acetone in steps of 50%, 50%, 100%, 100%, and 200% of the initial solution volume, with shaking at 1000 rpm for 5 minutes between additions. Samples were stored overnight at -20°C and centrifuged at 22,000×g for 30 minutes at 4°C. The dry pellet was then resuspended in 300 µL of 0.1% sodium deoxycholate (SDC) and 100 mM tris pH 8 using mechanical assistance (2 glass beads of 4 mm in a 2 mL tube at 1000 rpm for 2 hours).

Crosslinking Mass Spectrometry Sample Preparation

Digestion was carried out overnight at 37°C using trypsin from bovine pancreas (Merck) at a 1:20 enzyme/protein ratio. Trypsin activity was stopped by heating at 90°C for 10 minutes. To dephosphorylate endogenous peptides, the digested solution was supplemented with 25 mM $MgCl_2$, 50 mM KCl, and centrifuged at maximum speed for 5 minutes. The supernatant was separated, and the pellet was resuspended with 100 µL of 100 mM tris (pH 8). This solution underwent an additional centrifugation step to extract any remaining peptides, which were combined with the previous solution. Calf intestinal phosphatase (Quick CIP, NEB) at a concentration of 10 units/mL was added to the recovered supernatant, and it was incubated at 37°C for 8-10 hours.

Precipitation of residual SDC was induced by adjusting pH to 3 with formic acid. The solutions were then centrifuged to remove debris. Peptides were desalted using an Oasis HLB 96-well plate according to manufacturer's protocol (Waters Corporation). Cross-linked peptides were enriched using the MagReSyn® Zr-IMAC protocol (Resyn Biosciences) with minor adjustments compared to the manufacturer protocol, namely we used a beads:peptide ratio of 1:4 we increased the glycolic acid concentration to 1M in the binding buffer, and NH_3 to 5% in the elution buffer. Beads were recycled by repeating the entire protocol with the same nanoparticles for each sample and then joining the final eluates, as it was shown to increase the recovery (Bortel et al. 2024).

Mass Spectrometry Analysis (remember FAIMS)

Phospho-enriched peptides were processed in two different NanoLC-MS/MS configurations: a Dionex UltiMate 3000 RSLCnano coupled to an Orbitrap Exploris 480 through an FAIMS Pro™ interface (CV 55-60-75) (Thermo Fisher Scientific) and a UHPLC Vanquish Neo coupled to an Orbitrap Ascend Tribid mass spectrometer (Thermo Fisher Scientific). Peptides were separated on an Aurora Ultimate C18 column (IonOpticks) using a 120-minute gradient from 2.5% to 41% acetonitrile in 0.1% formic acid at 300 nL/min. Full scan MS spectra covered 400 to 1600 m/z. MS2 ions were fragmented with normalized collision energy of 21-28-36 for the Orbitrap Exploris and 21-29-37 for the Ascend. Ions with less than 2+ charge were excluded.

Evaluation of Monolink Abundance

Raw files were analyzed with FragPipe 22.0 (Kong et al. 2017) for modifications on lysine residues from PhoX. Isotopic masses considered were those of PhoX reacting with water (227.983 Da), ammonia (226.998 Da), and side derivatives (PhoX anhydride: 209.972 Da and PhoX-acetamide: 338.067 Da). The search was repeated with the identified proteins, this time seeking to identify semi-tryptic cleavage sites, which enabled the detection of amino terminal residues resulting from post-translational clevages and mature proteins after cleavage of the transit peptide.

Analysis of Crosslinked Peptides

For Crosslinks search data analysis was conducted using XlinkX Node in Proteome Discoverer 3.0 (Thermo Fisher Scientific) to identify cross-linked (XL) peptides with a minimum score cut-off of 40

(Klykov et al. 2018). The 20% most abundant identified proteins in the mono-link analysis (FragPipe output) were implemented as a database along with the inclusion of proteoforms with non-tryptic N-terminal cleavages. The proteoforms were obtained after including non-tryptic cleavage in FragPipe settings.

In order to conduct the study, only those cross-links that appeared in at least two out of three replicates (2 out 3) or all three replicates (3 out 3) for each condition were considered. Data filtering and formatting were conducted using an R script, which was subsequently employed to reshape the data into the input for xiNET, an online cross-link viewer developed by the Rappsilber Laboratory (Combe et al. 2015).

Custom R-Based Pipeline for Re-Annotation and Visualization of Cross-Linked Peptides in XiNET

To analyze cross-linked peptide data generated by Proteome Discoverer (PD), we developed a custom R-based pipeline for re-annotation and visualization of XL-peptides in xiNET. The analysis was performed using R version 4.2.1, incorporating packages such as tidyverse, dplyr, Biostrings, data.table, stringr, and seqinr. Input data consisted of crosslink spectrum matches (CSM) exported from PD and a reference protein sequence database.

The pipeline organized data according to MS run identifiers and classified them by experimental condition. Data pre-processing included filtering out cross-links that did not meet a user-defined minimum XlinkX score threshold (for this analysis 40) and grouping them based on a minimum number of repeated cross-link hits across replicates ("2 out of 3" and "3 out of 3" replicates). Remaining data were consolidated into unique cross-links, defined by sequence and site of crosslinking, retaining the highest score, the number of spectral matches, and the cumulative precursor abundances from aggregated CSMs. Cross-links were annotated with peptide sequences, linking positions, and associated scores, and formatted for visualization in xiNET.

Protein sequence re-annotation was performed by mapping peptides to a FASTA database, refining annotations originally assigned by PD This step aims to eliminate redundant proteoforms, essential for finding XLs with N-terminal residues after transient peptide cleavage. Furthermore, the pipeline generated all possible protein-pair combinations by aligning peptides to the updated database. This step is applied to distinguish between interactions that might occur between multiple proteins sharing the same peptide sequences due to high homology (e.g. light harvesting complex proteins), from protein-specific interactions. The complete R scripts used to handle the data are available at the GitHub repository https://github.com/LPM-team1/N-TRIMS

Author Contribution :

Conceptualization – NF, MF, GF, PA

Data Acquisition – NF, CG, PA

Data Analysis – NF, PA

Supervision – MF, GF, PA

Manuscript Writing - NF, MF, GF, PA

Acknowledgements

We would like to thank all the members of the LPM and EDyP laboratories for their support and assistance, especially A.M. Hesse, L. Belmudes, J. Novion-Ducassu, S. Kieffer-Jaquinod, S. Miesch-Frémyand and M. Menneteau for their invaluable technical support. This research project was funded by the 2022 ANR PRC program (PHOTO_DYN - 22-CE20-0015-01). P.A. acknowledges funding from the European Union's Horizon 2020 research and innovation program under the Marie Skłodowska-Curie grant agreement No 101066400 - PhotoLINK. GF acknowledge funding from the European Research Council ERC (Chloro-Mito; grant no. 833184) and the EIC PlanktON project (grant no. 101099192). Proteomic experiments were partially supported by Agence Nationale de la Recherche under projects ProFI (Proteomics French Infrastructure, ANR-10-INBS-08; ANR-24-INBS-0015). This work was also supported by ANR-17-EURE-0003 and GRAL and/or ANR-10-LABX-49-01

Data availability

All the raw data files are provided as Source Data to the corresponding figures. Code and scripts used to process and analyze fasta files and XL-MS data are accessible at the LPM GitHub repository https://github.com/LPM-team1 (N-TRIMS andxiNET-Mapping-Algorithm). All MS raw data files, including the search results, are deposited to the ProteomeXchange Consortium via the PRIDE partner repository (dataset identifier PXD068425)

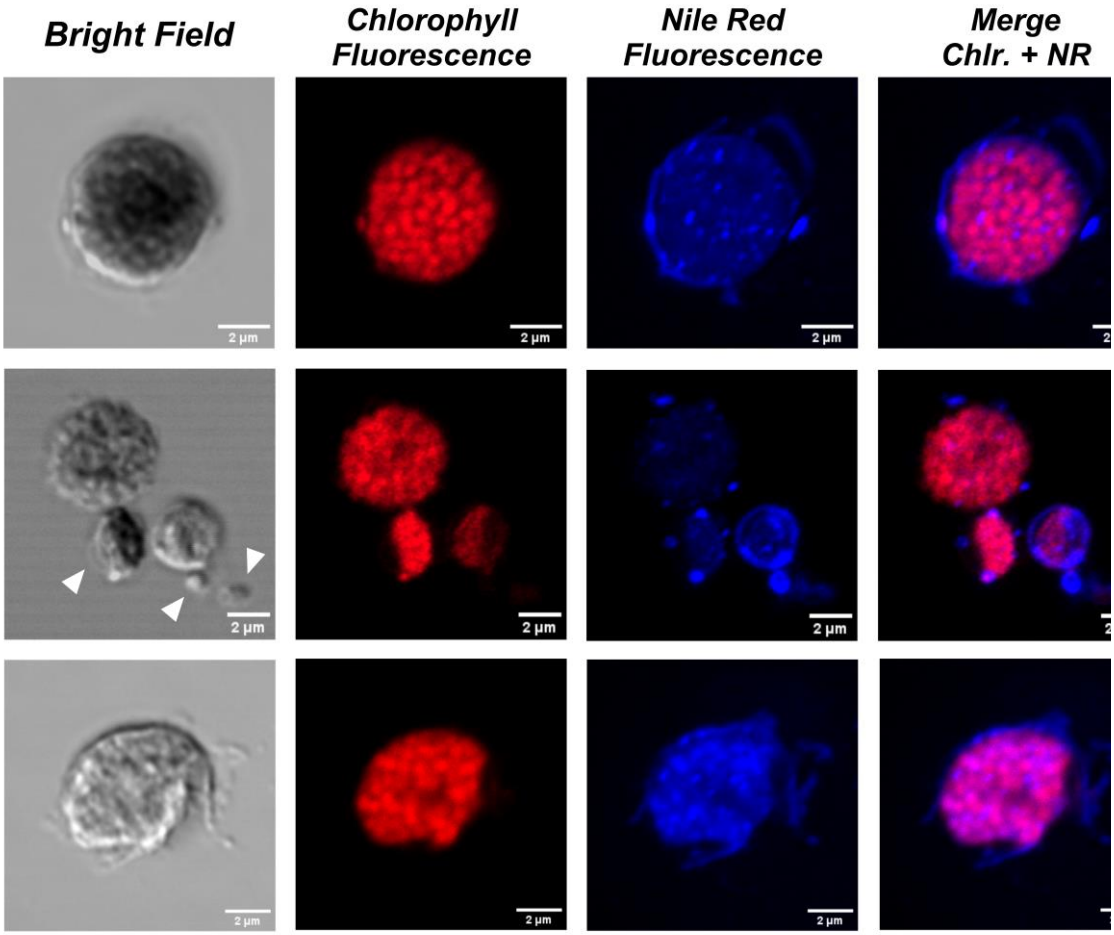

Figure S1. Confocal imaging of isolated thylakoid preparations. Representative bright-field and confocal fluorescence images showing chlorophyll autofluorescence (red) and Nile Red staining of membrane lipids (blue) in purified thylakoid membranes. Merged images highlight the overlap of chlorophyll and lipid fluorescence. Arrowheads indicate smaller membrane fragments visible in some preparations. Scale bars = 2 µm.

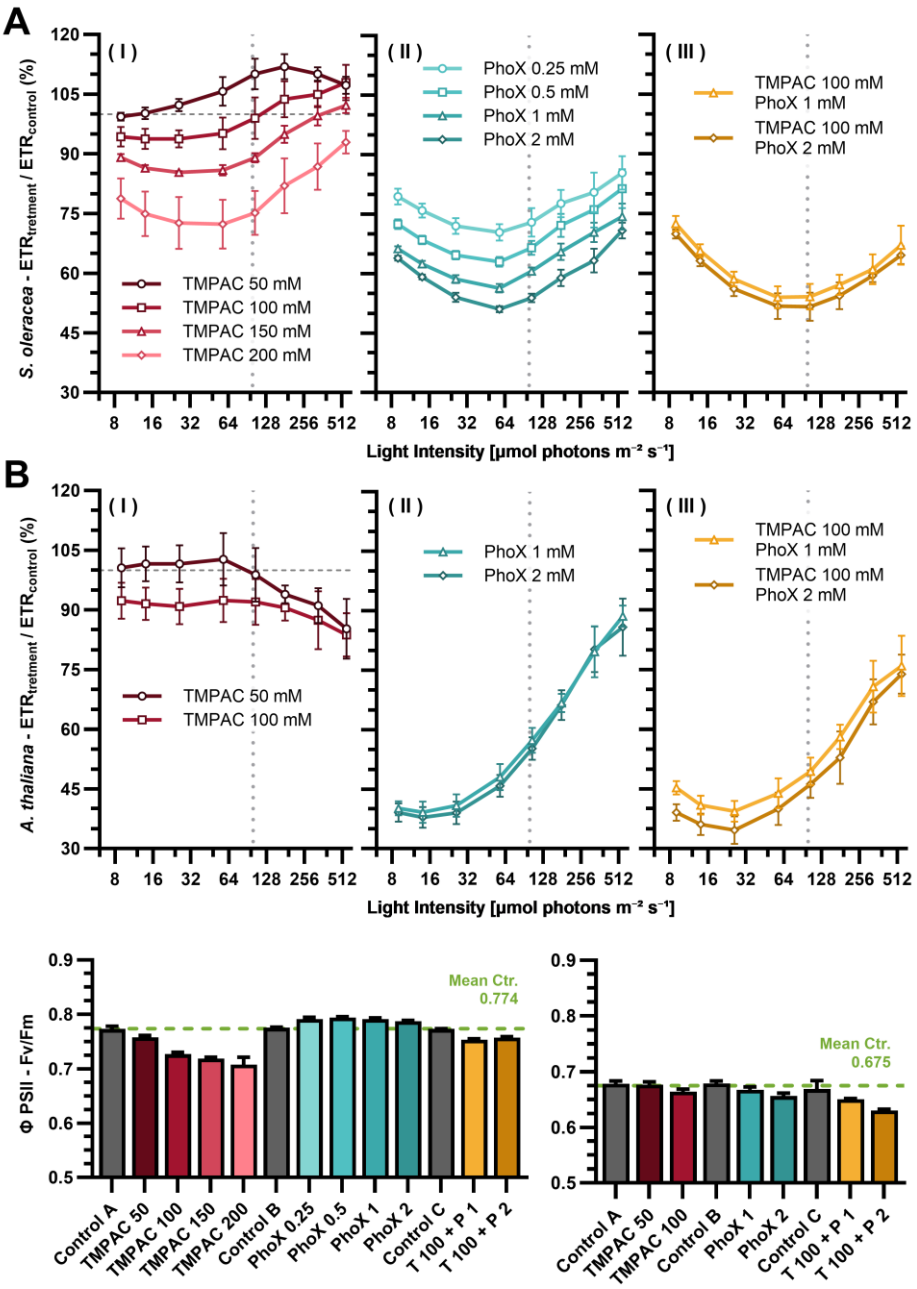

Figure S2. Photosynthetic performance in response to increasing TMPAC concentrations. A) Electron transport rate (ETR) values measured in Spinach thylakoids exposed to a concentration gradient of TMPAC (0 to 200 mM, I), Phox (0.25 to 2mM, II) and their combination to evaluate their addictive effect (III). B) Selected concentrations where tested also on Arabidopsis thyalkoids. TMPAC induces a modest dose-dependent decline in ETR, with minimal effects observed up to 100 mM. These results support 100 mM TMPAC as a functional working concentration that balances structural enhancement and physiological preservation. C) The maximum quantum yield of PSI was evaluated in dark-adapted samples for all the above-mentioned conditions. All measurements were done on at least 3 technical replicates (error bars st.dev. of minimum 3 replicates)

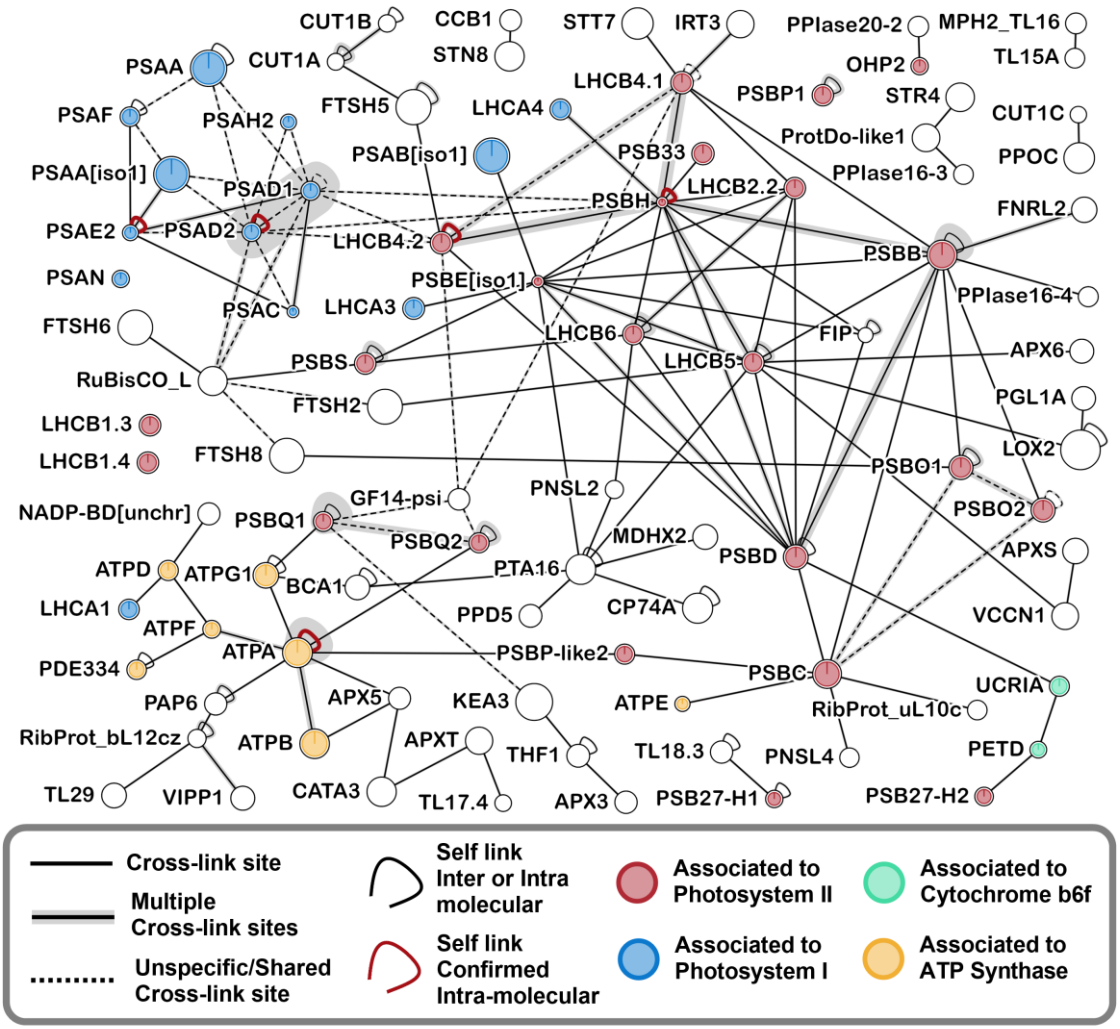

Figure S3 Interactome overview of thylakoids extracted from low-light acclimated *Arabidopsis thaliana* leaves (100 µmol photons m^{-2} s^{-1}) crosslinked with 1 mM of PhoX (with and without TMPAC). XLs present in at least 2 out of 3 replicas for each treatment are shown. Crosslink sites refers to dipeptides covalently bound; further details can be seen by opening the supplementary data S2 in the web application https://crosslinkviewer.org. Color coding of the proteins is based on the information available about their known interaction with photosynthetic complexes, or during their assembling. Due to the complexity of multi-interactions in LHCB antenna proteins, we highlighted them in grey to allow for a tidier visualization (full view of the interactome in Extended Data 1)

Table S1. Experimental conditions for crosslinking of thylakoid membranes. Growth light acclimation, crosslinker concentrations, TMPAC treatments, and sample-specific parameters for *Arabidopsis thaliana* (At) and *Spinacia oleracea* (So) thylakoid preparations. Values include maximum quantum yield of PSII (Fv/Fm, error <0.8%), total chlorophyll concentration, reaction volume, washing steps, protein-to-chlorophyll ratios, and total digested protein amounts.

Table S2. Annotated XL-MS data output across experimental conditions. Cross-linked peptide identifications from thylakoid samples of *Spinacia oleracea* (So) and *Arabidopsis thaliana* (At) under control (PhoX only) or TMPAC-treated conditions. Each sheet corresponds to one experimental setup: So_1mM_ctrl, So_1mM_TMPAC, So_2mM_ctrl, So_2mM_TMPAC, At_1mM_ctrl, At_1mM_TMPAC, At_2mM_ctrl, and At_2mM_TMPAC. Listing peptide sequences, crosslinking residues, protein assignments, replicate occurrence, and quantitative parameters (scores, spectral counts, precursor abundances). Additional annotation columns were appended to the original Proteome Discoverer software output table to provide functional information retrieved automatically from UniProt, including gene names, ORF identifiers, protein descriptions, annotated functions, GO/localization terms, and PDB codes with structural coverage, allowing mapping of crosslinks to known complexes.

Table S3. Structural mapping of identified crosslinks. Distance measurements for mapped crosslinks in available PDB structures of chloroplast complexes. Distances are reported as shortest Cα–Cα measurements, categorized per PDB entry and experimental condition, with indication of in-range (<35 Å) and out-of-range (>35 Å) values.

References

Abramson, Josh, Jonas Adler, Jack Dunger, et al. 2024. "Accurate Structure Prediction of Biomolecular Interactions with AlphaFold 3." *Nature* 630 (8016): 493–500. https://doi.org/10.1038/s41586-024-07487-w.

Albanese, Pascal, Sem Tamara, Guido Saracco, Richard A. Scheltema, and Cristina Pagliano. 2020. "How Paired PSII–LHCII Supercomplexes Mediate the Stacking of Plant Thylakoid Membranes Unveiled by Structural Mass-Spectrometry." *Nature Communications* 11 (1): 1361. https://doi.org/10.1038/s41467-020-15184-1.

Albanese, Pascal, Sem Tamara, Richard A. Scheltema, and Cristina Pagliano. 2020. "Structural Proteomics Applied to Plant Membrane Protein Complexes." *Trends in Plant Science* 25 (9): 945–46. https://doi.org/10.1016/j.tplants.2020.04.002.

Asada, Kozi. 1999. "THE WATER-WATER CYCLE IN CHLOROPLASTS: Scavenging of Active Oxygens and Dissipation of Excess Photons." *Annual Review of Plant Physiology and Plant Molecular Biology* 50 (June): 601–39. https://doi.org/10.1146/annurev.arplant.50.1.601.

Baird, B. A., and G. G. Hammes. 1976. "Chemical Cross-Linking Studies of Chloroplast Coupling Factor 1." *The Journal of Biological Chemistry* 251 (22): 6953–62.

Bar Barroeta, Awital, Pascal Albanese, Tereza Kadavá, et al. 2024. "Thrombin Activation of the Factor XI Dimer Is a Multistaged Process for Each Subunit." *Journal of Thrombosis and Haemostasis* 22 (5): 1336–46. https://doi.org/10.1016/j.jtha.2023.12.038.

Bassi, Roberto, and Luca Dall'Osto. 2021. "Dissipation of Light Energy Absorbed in Excess: The Molecular Mechanisms." *Annual Review of Plant Biology* 72 (June): 47–76. https://doi.org/10.1146/annurev-arplant-071720-015522.

Belsom, Adam, and Juri Rappsilber. 2021. “Anatomy of a Crosslinker.” *Current Opinion in Chemical Biology* 60 (February): 39–46. https://doi.org/10.1016/J.CBPA.2020.07.008.

Berentsen, Jarne, Peter R. Bos, and Emilie Wientjes. 2025. “Expansion Microscopy Reveals Thylakoid Organisation Alterations Due to Genetic Mutations and Far-Red Light Acclimation.” *Biochimica Et Biophysica Acta. Bioenergetics* 1866 (3): 149552. https://doi.org/10.1016/j.bbabio.2025.149552.

Blankenship, Robert E. 2010. “Early Evolution of Photosynthesis.” *Plant Physiology* 154 (2): 434–38. https://doi.org/10.1104/pp.110.161687.

Bludau, Isabell, and Ruedi Aebersold. 2020. “Proteomic and Interactomic Insights into the Molecular Basis of Cell Functional Diversity.” *Nature Reviews Molecular Cell Biology*, March 31, 1–14. https://doi.org/10.1038/s41580-020-0231-2.

Bortel, Patricia, Ilaria Piga, Claire Koenig, Christopher Gerner, Ana Martinez-Val, and Jesper V. Olsen. 2024. “Systematic Optimization of Automated Phosphopeptide Enrichment for High-Sensitivity Phosphoproteomics.” *Molecular & Cellular Proteomics* 23 (5): 100754. https://doi.org/10.1016/j.mcpro.2024.100754.

Bos, Peter R, Jarne Berentsen, and Emilie Wientjes. 2023. “Expansion Microscopy Resolves the Thylakoid Structure of Spinach.” *Plant Physiology*, October 4, kiad526. https://doi.org/10.1093/plphys/kiad526.

Bullock, Joshua Matthew Allen, Neeladri Sen, Konstantinos Thalassinos, and Maya Topf. 2018. “Modeling Protein Complexes Using Restraints from Crosslinking Mass Spectrometry.” *Structure*, July.

Burke, David F., Patrick Bryant, Inigo Barrio-Hernandez, et al. 2023. “Towards a Structurally Resolved Human Protein Interaction Network.” *Nature Structural & Molecular Biology* 30 (2): 216–25. https://doi.org/10.1038/s41594-022-00910-8.

Chavez, Juan D., Chi Fung Lee, Arianne Caudal, Andrew Keller, Rong Tian, and James E. Bruce. 2018. “Chemical Crosslinking Mass Spectrometry Analysis of Protein Conformations and Supercomplexes in Heart Tissue.” *Cell Systems* 6 (1): 136-141.e5. https://doi.org/10.1016/j.cels.2017.10.017.

Chavez, Juan D, Jared P Mohr, Martin Mathay, Xuefei Zhong, Andrew Keller, and James E Bruce. 2019. “Systems Structural Biology Measurements by in Vivo Cross-Linking with Mass Spectrometry.” *Nature Protocols* 14 (8): 2318–43. https://doi.org/10.1038/s41596-019-0181-3.

Combe, Colin W., Lutz Fischer, and Juri Rappsilber. 2015. “xiNET: Cross-Link Network Maps With Residue Resolution.” *Molecular & Cellular Proteomics* 14 (4): 1137–47. https://doi.org/10.1074/mcp.O114.042259.

Courteille, Agathe, Simona Vesa, Ruth Sanz-Barrio, et al. 2013. “Thioredoxin M4 Controls Photosynthetic Alternative Electron Pathways in Arabidopsis.” *Plant Physiology* 161 (1): 508–20. https://doi.org/10.1104/pp.112.207019.

Croce, Roberta, and Herbert van Amerongen. 2020. “Light Harvesting in Oxygenic Photosynthesis: Structural Biology Meets Spectroscopy.” *Science* 369 (6506). https://doi.org/10.1126/science.aay2058.

Dai, Shaodong, Rosmarie Friemann, Dominique A. Glauser, et al. 2007. “Structural Snapshots along the Reaction Pathway of Ferredoxin–Thioredoxin Reductase.” *Nature* 448 (7149): 92–96. https://doi.org/10.1038/nature05937.

Ditz, Noah, Hans-Peter Braun, and Holger Eubel. 2024. “Protein Assemblies in the Arabidopsis Thaliana Chloroplast Compartment.” *Frontiers in Plant Science* 15 (August): 1380969. https://doi.org/10.3389/fpls.2024.1380969.

Eberhard, Stephan, Giovanni Finazzi, and Francis-André Wollman. 2008. “The Dynamics of Photosynthesis.” *Annual Review of Genetics* 42 (1): 463–515. https://doi.org/10.1146/annurev.genet.42.110807.091452.

Fischer, N. 1998. “The PsaC Subunit of Photosystem I Provides an Essential Lysine Residue for Fast Electron Transfer to Ferredoxin.” *The EMBO Journal* 17 (4): 849–58. https://doi.org/10.1093/emboj/17.4.849.

Fristedt, Rikard, Inger Carlberg, Agnieszka Zygadlo, et al. 2009. “Intrinsically Unstructured Phosphoprotein TSP9 Regulates Light Harvesting in *Arabidopsis Thaliana*.” *Biochemistry* 48 (2): 499–509. https://doi.org/10.1021/bi8016334.

Giustini, Cécile, Davide Dal Bo, Mattia Storti, et al. 2025. “A Mitochondrially Derived Plastidial Transporter Regulates Photosynthesis in the Diatom *Phaeodactylum Tricornutum*.” Preprint, Plant Biology, February 18. https://doi.org/10.1101/2025.02.14.638225.

Gong, Xiao-Song, Jiang Qi Wen, Nicholas E. Fisher, et al. 2000. “The Role of Individual Lysine Residues in the Basic Patch on Turnip Cytochrome *f* for Electrostatic Interactions with Plastocyanin *in Vitro*.” *European Journal of Biochemistry* 267 (12): 3461–68. https://doi.org/10.1046/j.1432-1327.2000.01366.x.

Graziadei, Andrea, and Juri Rappsilber. 2022. “Leveraging Crosslinking Mass Spectrometry in Structural and Cell Biology.” *Structure* 30 (1): 37–54. https://doi.org/10.1016/j.str.2021.11.007.

Hansson, Maria, Tiphaine Dupuis, Ragna Strömquist, Bertil Andersson, Alexander V. Vener, and Inger Carlberg. 2007. “The Mobile Thylakoid Phosphoprotein TSP9 Interacts with the Light-Harvesting Complex II and the Peripheries of Both Photosystems.” *The Journal of Biological Chemistry* 282 (22): 16214–22. https://doi.org/10.1074/jbc.M605833200.

Henriques, Fernando, and Roderic B. Park. 1978. “Polypeptide Cross-Linking in Chloroplast Membranes.” *Archives of Biochemistry and Biophysics* 189 (1): 44–50. https://doi.org/10.1016/0003-9861(78)90112-1.

Hevler, Johannes F., Pascal Albanese, Alfredo Cabrera-Orefice, et al. 2023. “MRPS36 Provides a Structural Link in the Eukaryotic 2-Oxoglutarate Dehydrogenase Complex.” *Open Biology* 13 (3): 220363. https://doi.org/10.1098/rsob.220363.

Jumper, John, Richard Evans, Alexander Pritzel, et al. 2021. “Highly Accurate Protein Structure Prediction with AlphaFold.” *Nature 2021 596:7873* 596 (7873): 583–89. https://doi.org/10.1038/s41586-021-03819-2.

Kastritis, Panagiotis L, Francis J O’Reilly, Thomas Bock, et al. 2017. “Capturing Protein Communities by Structural Proteomics in a Thermophilic Eukaryote.” *Molecular Systems Biology* 13 (7): 936.

Kelley, Ron, Sagar Khavnekar, Ricardo D. Righetto, et al. 2024. “Towards Community-Driven Visual Proteomics with Large-Scale Cryo-Electron Tomography of *Chlamydomonas Reinhardtii*.” Preprint, December 28. https://doi.org/10.1101/2024.12.28.630444.

Klykov, Oleg, Mykhailo Kopylov, Bridget Carragher, Albert J.R. Heck, Alex J. Noble, and Richard A. Scheltema. 2022. “Label-Free Visual Proteomics: Coupling MS- and EM-Based Approaches in Structural Biology.” *Molecular Cell* 82 (2): 285–303. https://doi.org/10.1016/J.MOLCEL.2021.12.027.

Klykov, Oleg, Barbara Steigenberger, Sibel Pektaş, Domenico Fasci, Albert J. R. Heck, and Richard A. Scheltema. 2018. “Efficient and Robust Proteome-Wide Approaches for Cross-Linking Mass

Spectrometry." *Nature Protocols* 13 (12): 2964–90. https://doi.org/10.1038/s41596-018-0074-x.

Kong, Andy T, Felipe V Leprevost, Dmitry M Avtonomov, Dattatreya Mellacheruvu, and Alexey I Nesvizhskii. 2017. "MSFragger: Ultrafast and Comprehensive Peptide Identification in Mass Spectrometry–Based Proteomics." *Nature Methods* 14 (5): 513–20. https://doi.org/10.1038/nmeth.4256.

Liu, Fan, Philip Lössl, Beverley M. Rabbitts, RS Robert S. Balaban, and AJR Albert J.R. Heck. 2018. "The Interactome of Intact Mitochondria by Cross-Linking Mass Spectrometry Provides Evidence for Coexisting Respiratory Supercomplexes." *Molecular and Cellular Proteomics* 17 (2): 216–32. https://doi.org/10.1074/mcp.RA117.000470.

Lopes, Karina L., Ricardo A. O. Rodrigues, Marcos C. Silva, Wiliane G. S. Braga, and Marcio C. Silva-Filho. 2018. "The Zinc-Finger Thylakoid-Membrane Protein FIP Is Involved With Abiotic Stress Response in Arabidopsis Thaliana." *Frontiers in Plant Science* 9 (April): 504. https://doi.org/10.3389/fpls.2018.00504.

Maxwell, Kate, and Giles N. Johnson. 2000. "Chlorophyll Fluorescence - a Practical Guide." *Journal of Experimental Botany* (Univ Manchester, Sch Biol Sci, Manchester M13 9PT, Lancs, England. Univ Newcastle Upon Tyne, Dept Agr & Environm Sci, Environmm & Mol Plant Physiol Lab, Newcastle Upon Tyne NE1 7RU, Tyne & Wear, England.; Johnson, GN (reprint author), Univ Manchester, Sch) 51 (345): 659–68. https://doi.org/10.1093/jexbot/51.345.659.

McCafferty, Caitlyn L., Sven Klumpe, Rommie E. Amaro, Wanda Kukulski, Lucy Collinson, and Benjamin D. Engel. 2024. "Integrating Cellular Electron Microscopy with Multimodal Data to Explore Biology across Space and Time." *Cell* 187 (3): 563–84. https://doi.org/10.1016/j.cell.2024.01.005.

Mendes, Marta L, Lutz Fischer, Zhuo A Chen, et al. 2019. "An Integrated Workflow for Crosslinking Mass Spectrometry." *Molecular Systems Biology* 15 (9): e8994. https://doi.org/10.15252/msb.20198994.

Mosalaganti, Shyamal, Agnieszka Obarska-Kosinska, Marc Siggel, et al. 2022. "AI-Based Structure Prediction Empowers Integrative Structural Analysis of Human Nuclear Pores." *Science* 376 (6598): eabm9506. https://doi.org/10.1126/science.abm9506.

O'reilly, Francis J, and Juri Rappsilber. n.d. "Cross-Linking Mass Spectrometry: Methods and Applications in Structural, Molecular and Systems Biology." *Nature Structural & Molecular Biology*. https://doi.org/10.1038/s41594-018-0147-0.

O'Reilly, Francis J., Liang Xue, Andrea Graziadei, et al. 2020. "In-Cell Architecture of an Actively Transcribing-Translating Expressome." *Science* 369 (6503): 554–57. https://doi.org/10.1126/SCIENCE.ABB3758.

Ort, Donald R., Sabeeha S. Merchant, Jean Alric, et al. 2015. "Redesigning Photosynthesis to Sustainably Meet Global Food and Bioenergy Demand." *Proceedings of the National Academy of Sciences* 112 (28): 8529–36. https://doi.org/10.1073/pnas.1424031112.

Ray, Deepak K., Nathaniel D. Mueller, Paul C. West, and Jonathan A. Foley. 2013. "Yield Trends Are Insufficient to Double Global Crop Production by 2050." *PLoS ONE* 8 (6): e66428. https://doi.org/10.1371/journal.pone.0066428.

Sarewicz, Marcin, Mateusz Szwalec, Sebastian Pintscher, et al. 2023. "High-Resolution Cryo-EM Structures of Plant Cytochrome b_6 f at Work." *Science Advances* 9 (2): eadd9688. https://doi.org/10.1126/sciadv.add9688.

Schürmann, Peter, and Bob B. Buchanan. 2008. "The Ferredoxin/Thioredoxin System of Oxygenic Photosynthesis." *Antioxidants & Redox Signaling* 10 (7): 1235–74. https://doi.org/10.1089/ars.2007.1931.

Steigenberger, B., P. Albanese, A. J.R. Heck, and R. A. Scheltema. 2020. "To Cleave or Not to Cleave in XL-MS?" *Journal of the American Society for Mass Spectrometry* 31 (2): 196–206. https://doi.org/10.1021/jasms.9b00085.

Weisz, Daniel A., Haijun Liu, Hao Zhang, et al. 2017. "Mass Spectrometry-Based Cross-Linking Study Shows That the Psb28 Protein Binds to Cytochrome b_{559} in Photosystem II." *Proceedings of the National Academy of Sciences* 114 (9): 2224–29. https://doi.org/10.1073/pnas.1620360114.

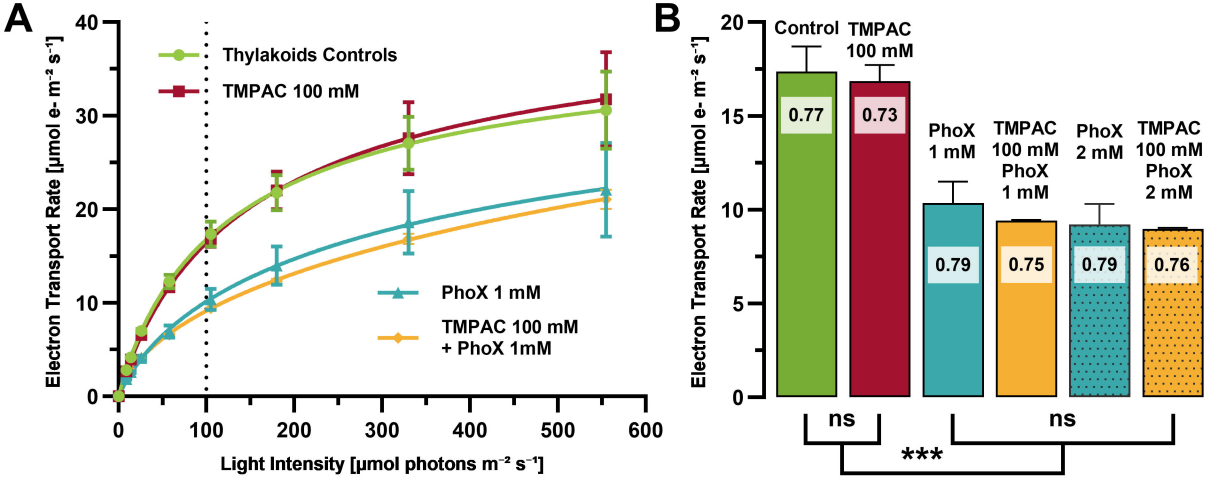
A
Electron Transport Rate [µmol e- m⁻² s⁻¹]
Light Intensity [µmol photons m⁻² s⁻¹]
Thylakoids Controls
TMPAC 100 mM
PhoX 1 mM
TMPAC 100 mM
+ PhoX 1mM
B
Control
TMPAC 100 mM
PhoX 1 mM
TMPAC 100 mM PhoX 1 mM
PhoX 2 mM
TMPAC 100 mM PhoX 2 mM
0.77
0.73
0.79
0.75
0.79
0.76
ns
ns
***

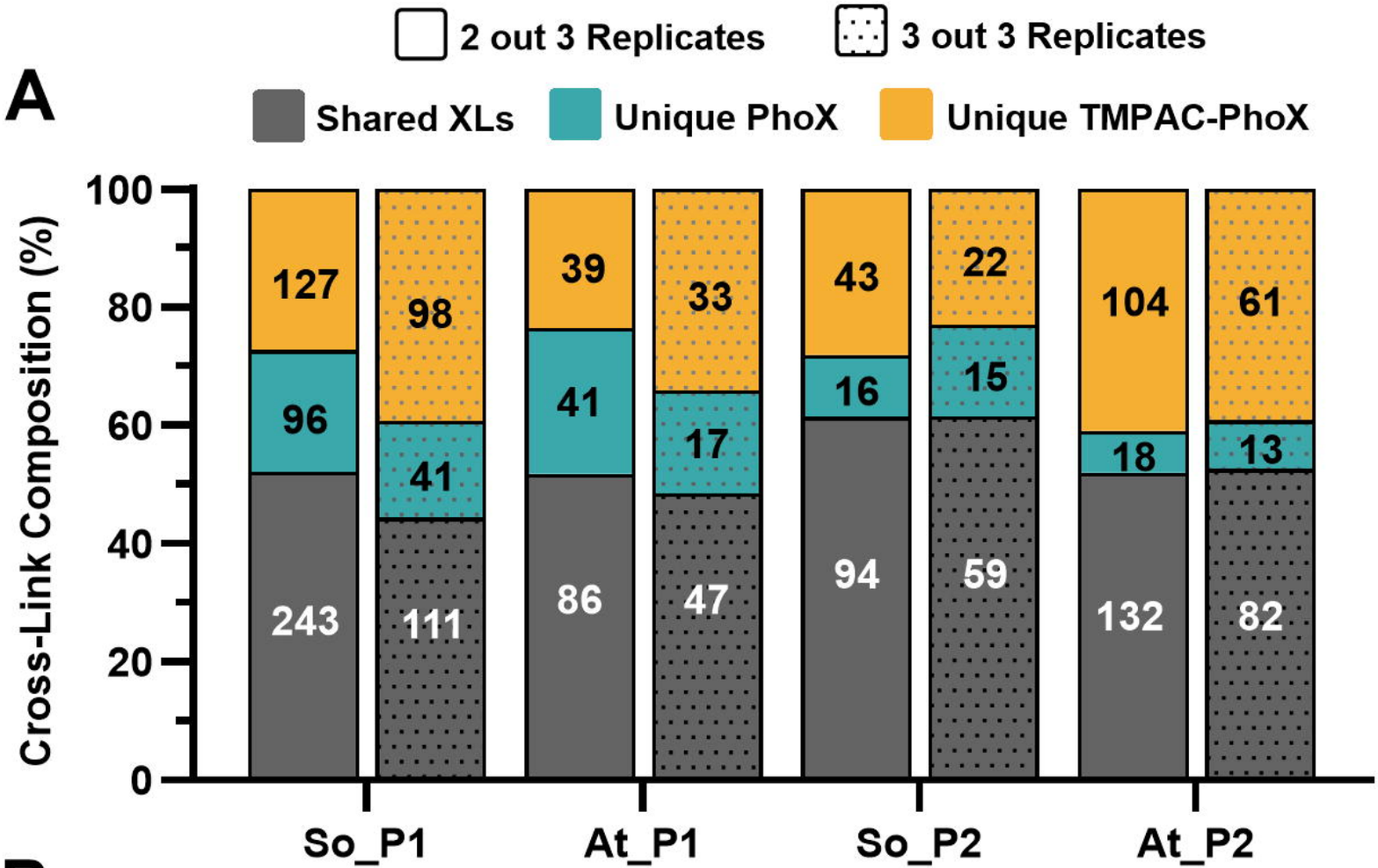
A
2 out 3 Replicates
3 out 3 Replicates
Shared XLs
Unique PhoX
Unique TMPAC-PhoX
Cross-Link Composition (%)
100
80
60
40
20
0
127
96
243
98
41
111
39
41
86
33
17
47
43
16
94
22
15
59
104
18
132
61
13
82
So_P1
At_P1
So_P2
At_P2

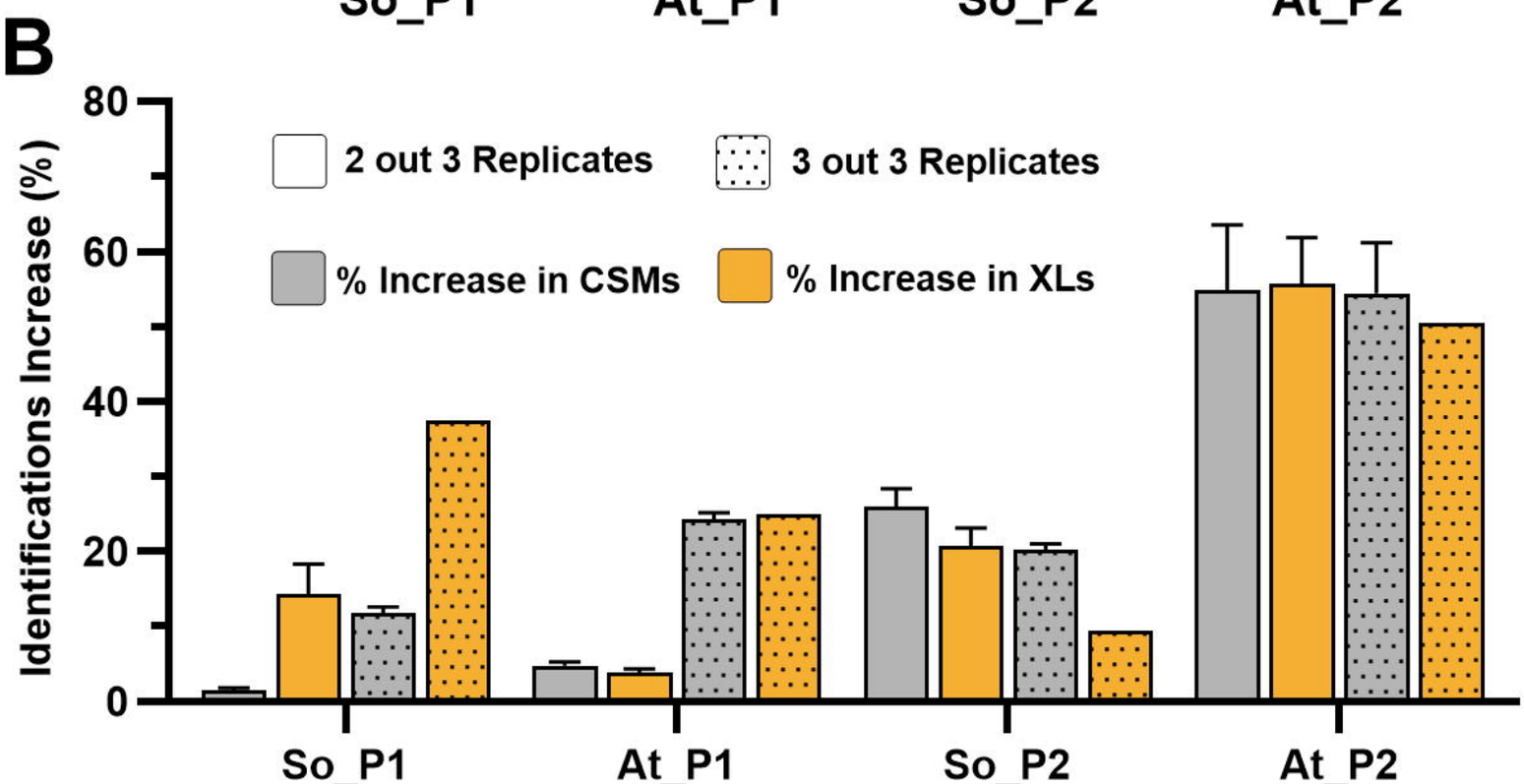
B
Identifications Increase (%)
80
60
40
20
0
2 out 3 Replicates
3 out 3 Replicates
% Increase in CSMs
% Increase in XLs
So_P1
At_P1
So_P2
At_P2

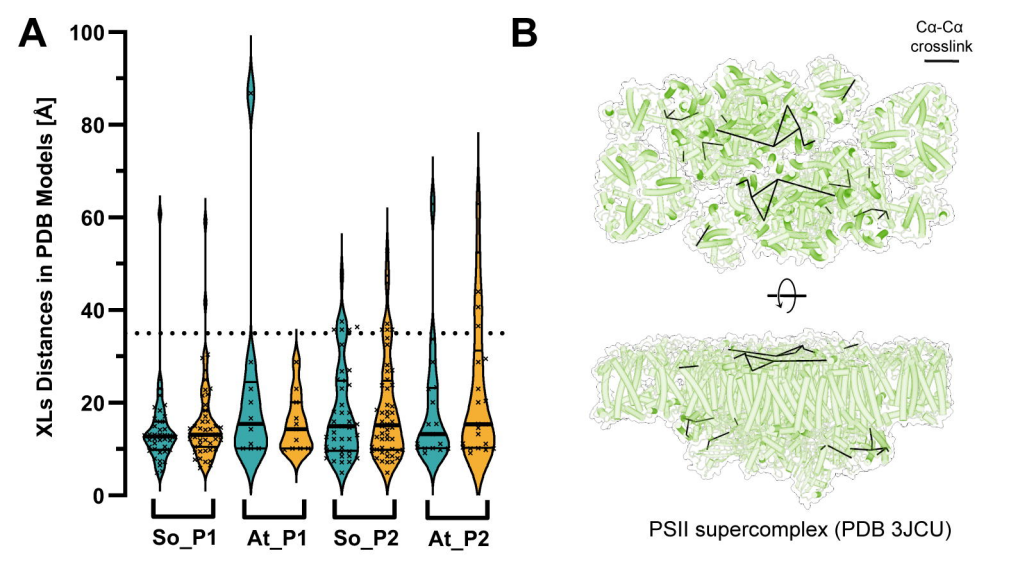
A
B
XLs Distances in PDB Models [Å]
100
80
60
40
20
0
So_P1
At_P1
So_P2
At_P2
Cα-Cα
crosslink
PSII supercomplex (PDB 3JCU)

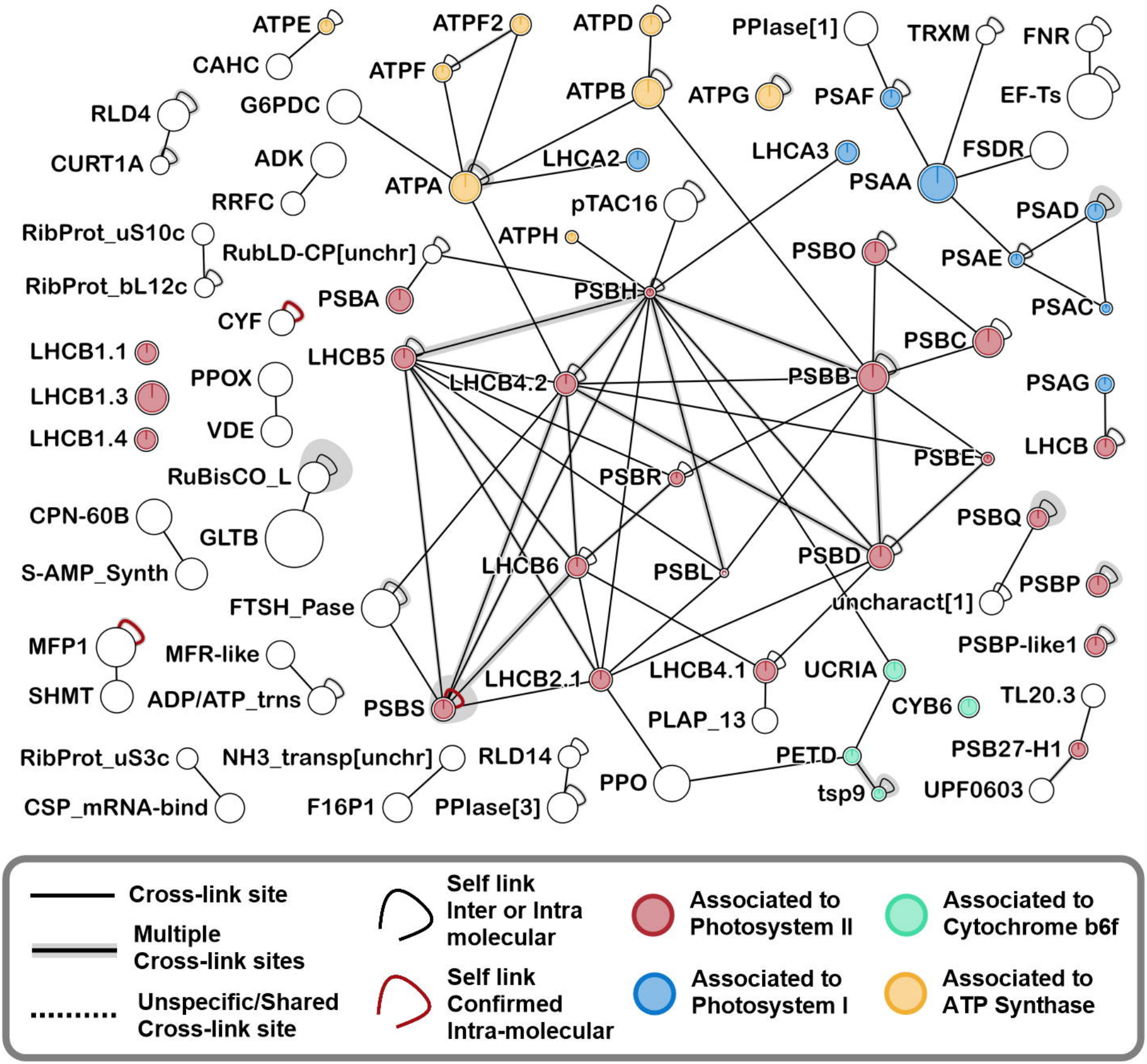
ATPE
ATPF2
ATPD
PPIase[1]
TRXM
FNR
CAHC
ATPF
ATPB
ATPG
PSAF
EF-Ts
RLD4
G6PDC
CURT1A
ADK
LHCA2
LHCA3
FSDR
ATPA
PSAA
RRFC
pTAC16
PSAD
RibProt_uS10c
ATPH
RubLD-CP[unchr]
PSBO
PSAE
RibProt_bL12c
PSBA
PSBH
PSAC
CYF
PSBC
LHCB1.1
LHCB5
PPOX
LHCB4.2
PSBB
PSAG
LHCB1.3
VDE
LHCB1.4
PSBE
LHCB
RuBisCO_L
PSBR
CPN-60B
PSBQ
GLTB
PSBD
S-AMP_Synth
LHCB6
PSBL
PSBP
FTSH_Pase
uncharact[1]
MFP1
MFR-like
PSBP-like1
LHCB2.1
LHCB4.1
UCRIA
SHMT
ADP/ATP_trns
PSBS
CYB6
TL20.3
PLAP_13
RibProt_uS3c
NH3_transp[unchr]
RLD14
PETD
PSB27-H1
PPO
tsp9
UPF0603
CSP_mRNA-bind
F16P1
PPIase[3]
Cross-link site
Multiple Cross-link sites
Unspecific/Shared Cross-link site
Self link Inter or Intra molecular
Self link Confirmed Intra-molecular
Associated to Photosystem II
Associated to Photosystem I
Associated to Cytochrome b6f
Associated to ATP Synthase

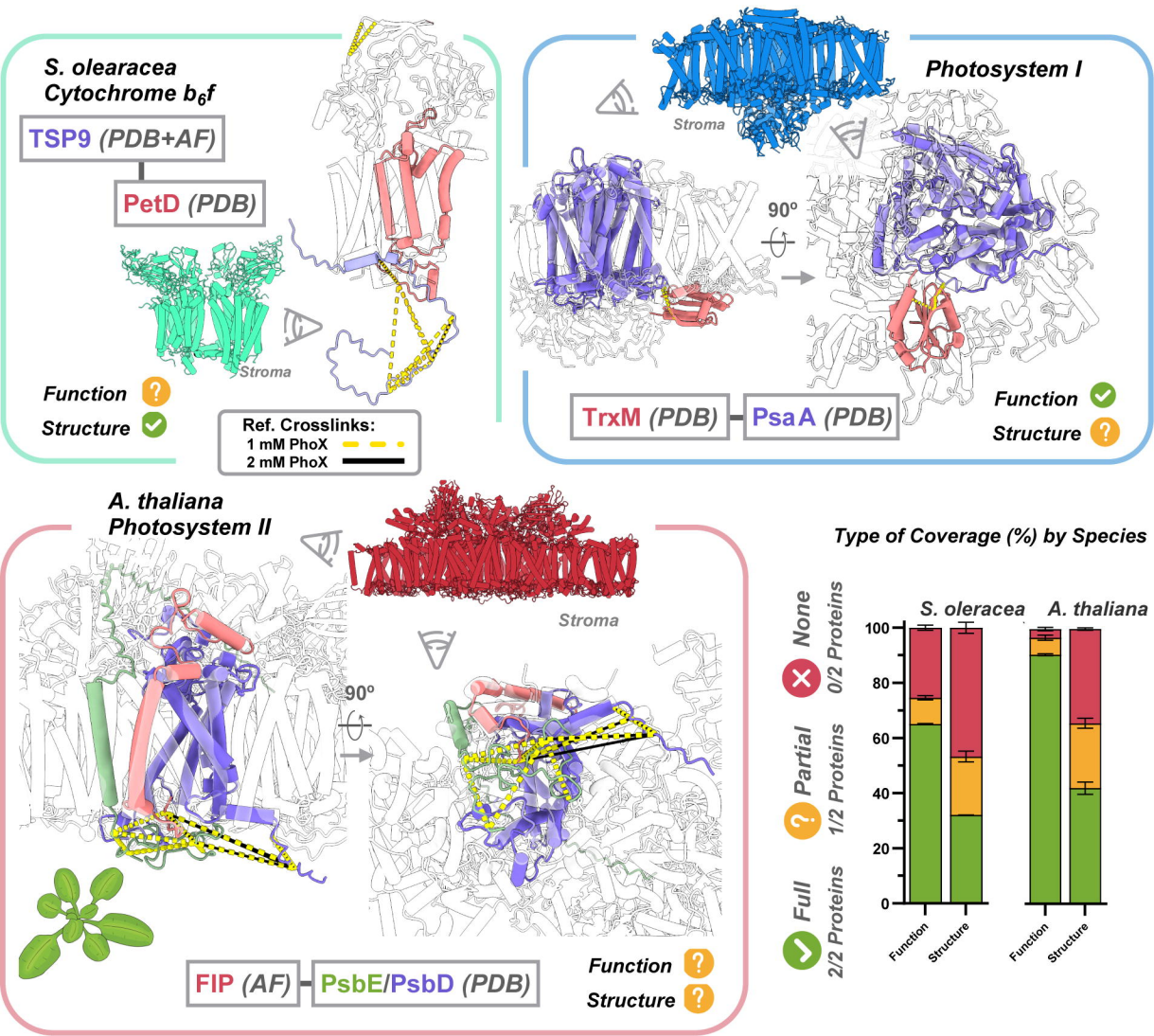
S. olearacea
Cytochrome b6f
TSP9 (PDB+AF)
PetD (PDB)
Stroma
Function
Structure
Ref. Crosslinks:
1 mM PhoX
2 mM PhoX
Photosystem I
Stroma
90°
TrxM (PDB)
PsaA (PDB)
Function
Structure
A. thaliana
Photosystem II
Stroma
90°
FIP (AF)
PsbE/PsbD (PDB)
Function
Structure
Type of Coverage (%) by Species
None
0/2 Proteins
Partial
1/2 Proteins
Full
2/2 Proteins
S. oleracea
A. thaliana
100
80
60
40
20
0
Function
Structure
Function
Structure

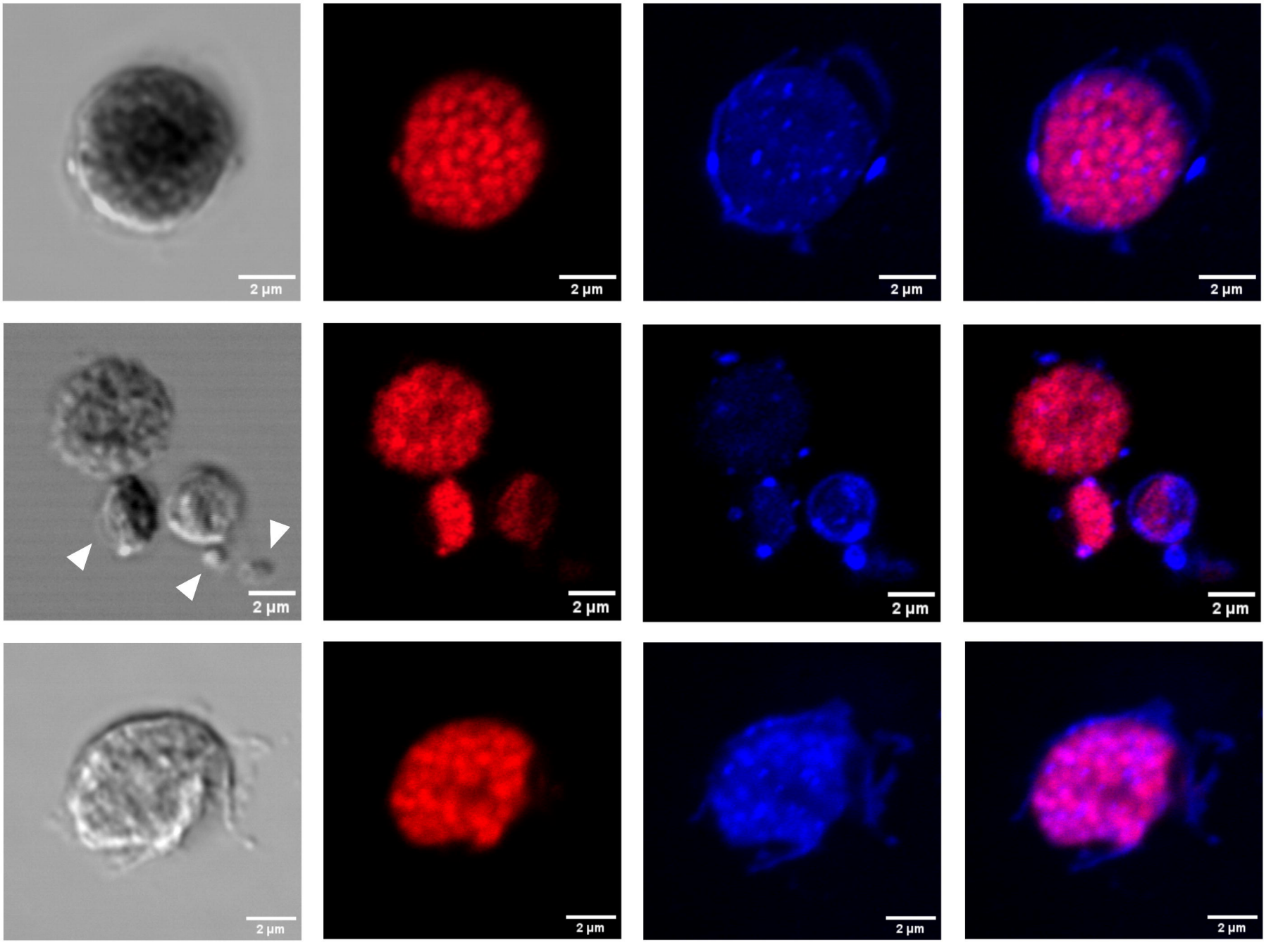
Bright Field
Chlorophyll Fluorescence
Nile Red Fluorescence
Merge Chlr. + NR
2 µm

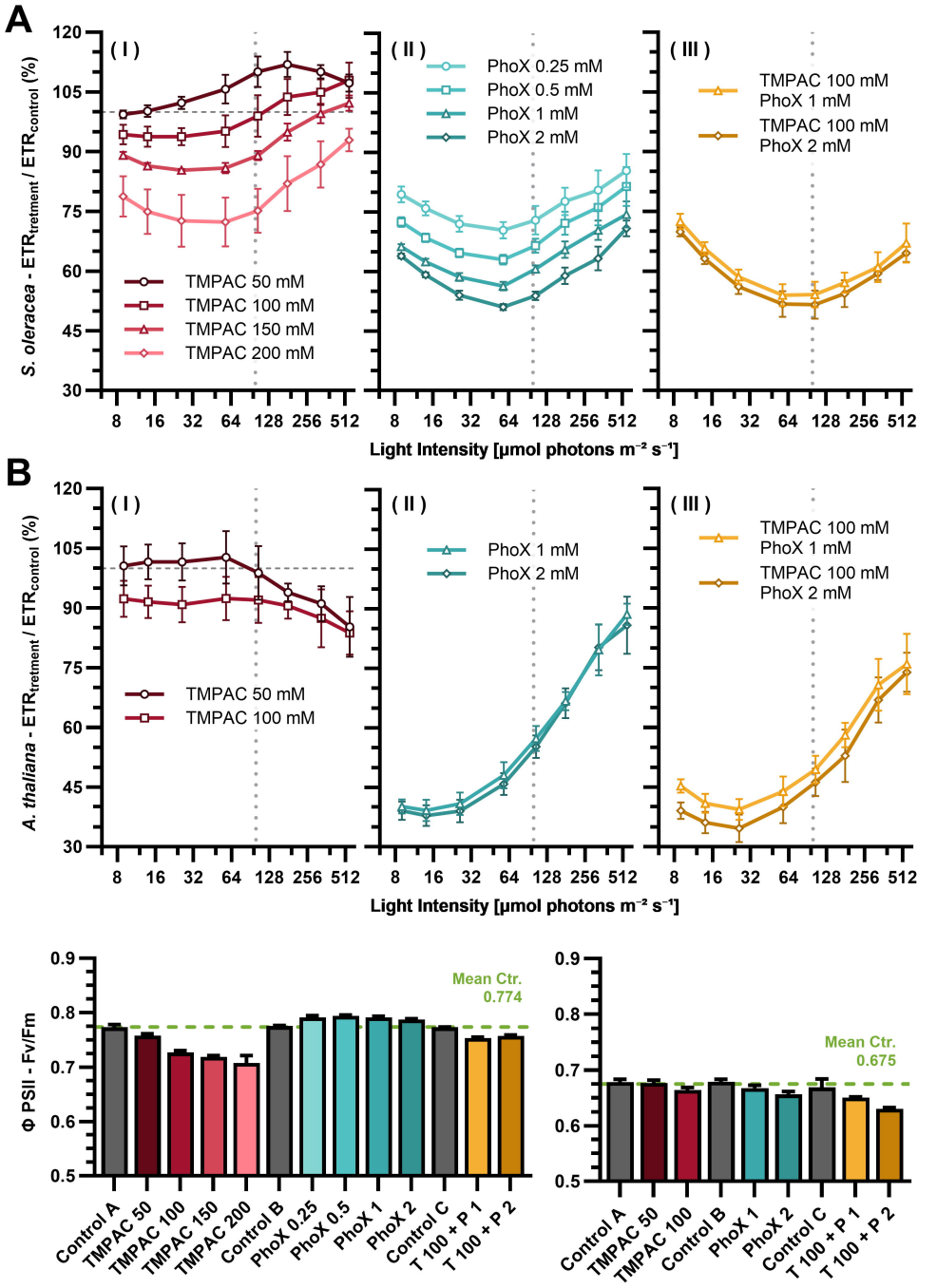
A
(I)
(II)
(III)
S. oleracea - ETRtretment / ETRcontrol (%)
TMPAC 50 mM
TMPAC 100 mM
TMPAC 150 mM
TMPAC 200 mM
PhoX 0.25 mM
PhoX 0.5 mM
PhoX 1 mM
PhoX 2 mM
TMPAC 100 mM
PhoX 1 mM
TMPAC 100 mM
PhoX 2 mM
Light Intensity [µmol photons m⁻² s⁻¹]
B
A. thaliana - ETRtretment / ETRcontrol (%)
Light Intensity [µmol photons m⁻² s⁻¹]
Φ PSII - Fv/Fm
Mean Ctr.
0.774
Mean Ctr.
0.675
Control A
TMPAC 50
TMPAC 100
TMPAC 150
TMPAC 200
Control B
PhoX 0.25
PhoX 0.5
PhoX 1
PhoX 2
Control C
T 100 + P 1
T 100 + P 2

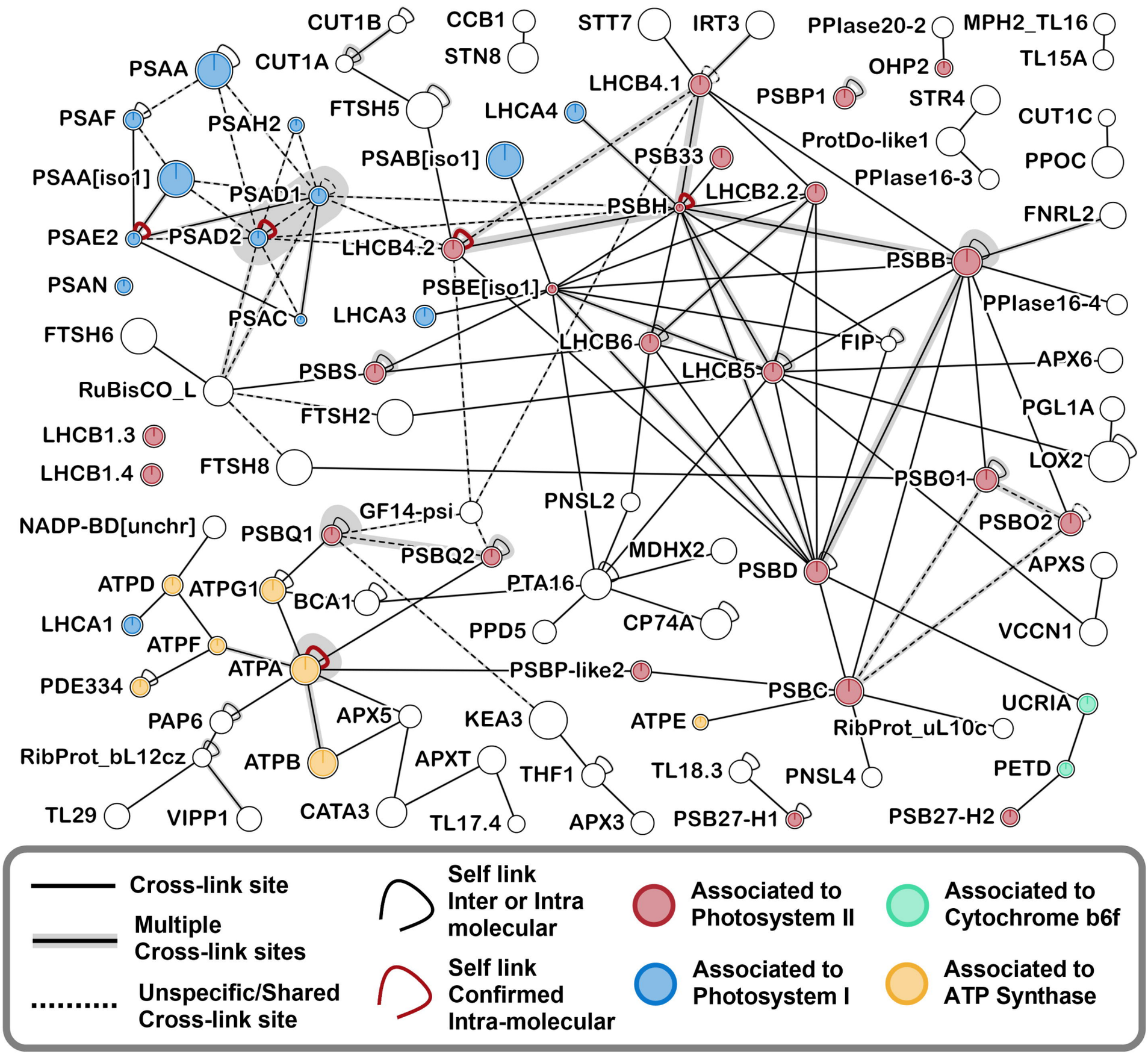
CUT1B
CCB1
STT7
IRT3
PPIase20-2
MPH2_TL16
STN8
OHP2
TL15A
PSAA
CUT1A
LHCB4.1
PSBP1
STR4
PSAF
PSAH2
FTSH5
LHCA4
CUT1C
ProtDo-like1
PSAB[iso1]
PSB33
PPOC
PSAA[iso1]
PSAD1
PPIase16-3
LHCB2.2
PSBH
FNRL2
PSAE2
PSAD2
LHCB4.2
PSBB
PSAN
PSBE[iso1]
PPIase16-4
PSAC
LHCA3
FTSH6
LHCB6
FIP
APX6
PSBS
LHCB5
RuBisCO_L
PGL1A
FTSH2
LHCB1.3
LOX2
LHCB1.4
FTSH8
PSBO1
PNSL2
GF14-psi
NADP-BD[unchr]
PSBQ1
PSBO2
PSBQ2
MDHX2
PSBD
APXS
ATPD
ATPG1
BCA1
PTA16
LHCA1
PPD5
CP74A
VCCN1
ATPF
ATPA
PSBP-like2
PDE334
PSBC
UCRIA
PAP6
APX5
KEA3
ATPE
RibProt_uL10c
RibProt_bL12cz
ATPB
APXT
THF1
TL18.3
PNSL4
PETD
TL29
VIPP1
CATA3
TL17.4
APX3
PSB27-H1
PSB27-H2
Cross-link site
Multiple Cross-link sites
Unspecific/Shared Cross-link site
Self link Inter or Intra molecular
Self link Confirmed Intra-molecular
Associated to Photosystem II
Associated to Photosystem I
Associated to Cytochrome b6f
Associated to ATP Synthase